IEEE Open Journal of
Antennas and Propagation

Received 20 February 2021; accepted 21 March 2021. Date of publication 31 March 2021; date of current version 16 April 2021.

Digital Object Identifier 10.1109/OJAP.2021.3070199

Analysis of Interaction Scattering Cross Sections and Their Physical Bounds for Multiple-Dipole Stimulation of a Three-Dimensional Layered Medium

ANDREAS KALOGEROPOULOS AND NIKOLAOS L. TSITSAS (Senior Member, IEEE)

School of Informatics, Aristotle University of Thessaloniki, 54124 Thessaloniki, Greece

CORRESPONDING AUTHOR: N. L. TSITSAS (e-mail: ntsitsas@csd.auth.gr)

ABSTRACT A three-dimensional layered and isotropic medium is excited by primary spherical waves due to N magnetic dipoles radiating inside or outside the medium. Interaction scattering cross sections (ISCS) are defined as the differences between the overall scattering cross section and the sum of the individual cross sections generated by all dipoles within a layer or by all N dipoles. Optical theorems and physical bounds for the ISCS are established. Extensive numerical investigations are performed for the variations of the ISCS and their physical bounds with respect to the geometrical and physical characteristics of the layered medium. Conditions for which ISCS contribute significantly in the overall cross section are analyzed. It is also demonstrated that the number of excitation layers and the total number N of dipoles can be determined by means of the individual scattering cross sections.

INDEX TERMS Electromagnetic scattering, layered medium, dipoles, physical bounds, scattering cross sections.

I. INTRODUCTION

EXCITATION of a three-dimensional layered (piecewise homogeneous) medium by N electric or magnetic dipoles, located in different internal layers or in the medium's exterior, constitutes a realistic model for applications spreading from low frequencies to the visible range. Representative applications include, e.g., stimulation of the brain by the neurons currents [1], [2], cancer-treatment techniques like ablation and interstitial hyperthermia [3], [4], radiation by multiple sensors in 5G networks [5], multilayer optical diffusion [6], and design of nonplanar microstrip antennas [7]. Moreover, in the context of inverse problems, excitation by N dipoles was employed in field-splitting techniques [8], identifications of fields on spherically-symmetric conductors [9], reconstruction of obstacles buried in layered media [10], and dipoles localization using electromagnetic induction sensors [11]. Besides, scattering by layered uniaxial objects was investigated in [12] by employing a methodology involving electric and magnetic infinitesimal dipoles located in different layers.

In this work, we, first, formulate the boundary-value problems for the generated electric fields corresponding to the excitation of a piecewise homogeneous medium composed of annuli-like layers by N internal and external magnetic dipoles. Then, we adopt specific fields' decompositions and introduce interaction scattering cross sections (ISCS) as the differences between the overall scattering cross section and the sum of the individual cross sections due to all dipoles of a certain layer or due to all N dipoles exciting the scatterer. ISCS quantify the energy flux rate which is induced by the interaction of the individual fields and is not directly connected to an actual dipole involved in the boundary-value problem.

Next, we distinguish two different cases: *single-layer excitation* when all dipoles lie in the same layer (or in the medium's exterior) and *mixed excitation* when dipoles are located in more than one layers. For each of the two cases, we derive optical theorems determining the individual and overall scattering cross sections by means of the secondary fields at the dipoles' positions. Optical theorems relating the ISCS with the partial fields (defined as the sum of the individual fields due to all dipoles in an excitation layer except one) are also established. Moreover, we derive physical bounds for the ISCS with respect to the minimum and maximum

individual cross sections and the numbers of dipoles and excitation layers.

Several numerical results are presented demonstrating the variations of the ISCS and their associated physical bounds with respect to the physical and geometrical characteristics of the layered medium as well as the numbers and locations of the dipoles. By performing extensive parametric analyses, we point out scattering configurations and conditions in which the ISCS contribute significantly in the overall cross section; clarifying this is important when examining the additivity of the scattering cross sections. Mainly for mixed-excitation, it is shown that the ISCS become negative in some cases, which means that fields interactions reduce the expected energy flux rate. Furthermore, changing the materials of the layers affects significantly the ISCS in mixed excitation, but does not result in significant variations in single-layer excitation. The influence on the ISCS of the excitation dipoles' distance from the medium's boundary is also analyzed. Additionally, it is shown that the number of excitation layers and the total number N of dipoles can be determined by the derived physical bounds involving the individual scattering cross sections. It is also demonstrated that for external excitation the ISCS ratios in the low-frequency regime are very close to $1-\frac{1}{N}$.

This paper is organized as follows. The formulation of the boundary-value problems and the definitions of the ISCS are included in Section II. Optical theorems and physical bounds on the ISCS together with numerical results with respect to changes in the layered medium and the excitation dipoles are presented in Sections III and IV, for the single-layer and mixed excitation cases, respectively. Selected conclusions from the numerical results are summarized in Section V.

II. MATHEMATICAL FORMULATION

The considered three-dimensional layered medium V is shown in Fig. 1. It has a $\mathcal{C}^2$ boundary S_1 and is divided by $P-1$ $\mathcal{C}^2$ surfaces S_p $(p=2,\ldots,P)$ into P annuli-like layers V_p $(p=1,\ldots,P)$. Surface S_p includes surfaces S_q, for all $q>p$ and $p=1,\ldots,P$. The first $P-1$ layers V_p are homogeneous, isotropic and dielectric with real wavenumbers k_p, dielectric permittivities ϵ_p, and magnetic permeabilities μ_p. The scatterer's core V_P can be a perfect electric conductor (PEC), perfect magnetic conductor (PMC) or isotropic dielectric with wavenumber k_P, permittivity ϵ_P, and permeability μ_P. The exterior V_0 of V has respective physical parameters k_0, ϵ_0, and μ_0.

The layered medium V is excited by N magnetic dipoles which are distributed arbitrarily in its interior or its exterior. These N dipoles are located at $\mathbf{r}^i$ and possess unit dipole moments $\hat{\mathbf{p}}^i$, with $i=1,\ldots,N$. In particular, we suppose that the dipoles are contained in Q of the medium's layers, called *excitation layers* and denoted by V_q^{ex}, with $Q\leq P+1$. When dipoles lie in V_0, then V_1^{ex} (for $q=1$) coincides with V_0. Each excitation layer V_q^{ex} contains n_q dipoles, of strength A_q^j, position vector $\mathbf{r}_q^j$, and dipole moment $\hat{\mathbf{p}}_q^j$, for $j=1,\ldots,n_q$. Hence, it holds that $n_1+n_2+\cdots+n_Q=N$.

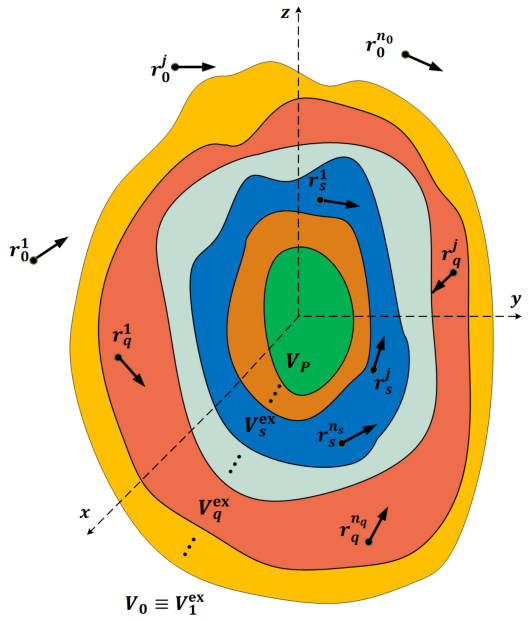

FIGURE 1. The considered three-dimensional piecewise-homogeneous medium composed of annuli-like layers and stimulated by N (external and internal) magnetic dipoles.

Each magnetic dipole radiates a primary electric field (under an $\exp(-\mathrm{i}\omega t)$ time dependence with ω as the angular frequency, t as time, and $\mathrm{i}=\sqrt{-1}$)

$$\mathbf{E}^{\mathrm{pr}}\left(\mathbf{r};\mathbf{r}_q^j\right)=A_q^j\nabla\times\left(\frac{\exp\left(\mathrm{i}k_q\left|\mathbf{r}-\mathbf{r}_q^j\right|\right)}{\left|\mathbf{r}-\mathbf{r}_q^j\right|}\hat{\mathbf{p}}_q^j\right),\quad \mathbf{r}\neq\mathbf{r}_q^j, \tag{1}$$

where $j=1,\ldots,n_q$ and $q=1,\ldots,Q$. According to the scattering superposition method [13], [14], the total electric field in V_q^{ex} due to a dipole at $\mathbf{r}_q^j\in V_q^{\mathrm{ex}}$ is expressed as

$$\mathbf{E}_q^{\mathrm{t}}\left(\mathbf{r};\mathbf{r}_q^j\right)=\mathbf{E}^{\mathrm{pr}}\left(\mathbf{r};\mathbf{r}_q^j\right)+\mathbf{E}_q^{\mathrm{sec}}\left(\mathbf{r};\mathbf{r}_q^j\right),\quad \mathbf{r}\in V_q^{\mathrm{ex}}\backslash\left\{\mathbf{r}_q^j\right\}, \tag{2}$$

where $\mathbf{E}_p^{\mathrm{sec}}(\mathbf{r};\mathbf{r}_q^j)$ is the secondary field in layer V_p due to a dipole at $\mathbf{r}_q^j$. If V_p is not an excitation layer, then $\mathbf{E}_p^{\mathrm{t}}(\mathbf{r};\mathbf{r}_q^j)=\mathbf{E}_p^{\mathrm{sec}}(\mathbf{r};\mathbf{r}_q^j)$. Fields due to a single excitation dipole will be referred to as *individual fields*.

Next, we define the *secondary* and *total q-excitation fields* as the superpositions of the corresponding individual fields due to all dipoles in V_q^{ex}, i.e.,

$$\mathbf{E}_p^{\ell}\left(\mathbf{r};\mathbf{r}_q^1,\ldots,\mathbf{r}_q^{n_q}\right)=\sum_{j=1}^{n_q}\mathbf{E}_p^{\ell}\left(\mathbf{r};\mathbf{r}_q^j\right), \tag{3}$$

where $\ell\in\{\mathrm{sec},\mathrm{t}\}$. If V_p is an excitation layer V_q^{ex}, then the *q-excitation field* is given by

$$\begin{aligned}&\mathbf{E}_q^{\mathrm{t}}\left(\mathbf{r};\mathbf{r}_q^1,\ldots,\mathbf{r}_q^{n_q}\right)\\&=\mathbf{E}^{\mathrm{pr}}\left(\mathbf{r};\mathbf{r}_q^1,\ldots,\mathbf{r}_q^{n_q}\right)\\&\quad+\mathbf{E}_q^{\mathrm{sec}}\left(\mathbf{r};\mathbf{r}_q^1,\ldots,\mathbf{r}_q^{n_q}\right),\quad \mathbf{r}\in V_q^{\mathrm{ex}}\backslash\left\{\mathbf{r}_q^1,\ldots,\mathbf{r}_q^{n_q}\right\},\end{aligned} \tag{4}$$

where the *primary q-excitation field* is defined as

$$\mathbf{E}^{\mathrm{pr}}\left(\mathbf{r};\mathbf{r}_q^1,\ldots,\mathbf{r}_q^{n_q}\right)=\sum_{j=1}^{n_q}\mathbf{E}^{\mathrm{pr}}\left(\mathbf{r};\mathbf{r}_q^j\right). \tag{5}$$

The *overall secondary* $\mathbf{E}_p^{\mathrm{sec}}(\mathbf{r};\mathbf{r}^1,\ldots,\mathbf{r}^N)$ and *overall total field* $\mathbf{E}_p^{\mathrm{t}}(\mathbf{r};\mathbf{r}^1,\ldots,\mathbf{r}^N)$ of V_p are defined, accordingly, as the superpositions of *all* corresponding fields due to all N dipoles.

Individual, q-excitation, and overall fields satisfy the vector Helmholtz equations

$$\nabla^2\mathbf{E}_p^{\mathrm{t}}(\mathbf{r};\cdot)+k_p^2\mathbf{E}_p^{\mathrm{t}}(\mathbf{r};\cdot)=\mathbf{0}, \tag{6}$$

in V_p, if V_p is not an excitation layer, and in $V_q^{\mathrm{ex}}\backslash\{\mathbf{r}_q^1,\ldots,\mathbf{r}_q^{n_q}\}$ if V_p is an excitation layer V_q^{ex}. These fields also satisfy the transmission conditions

$$\hat{\mathbf{n}}\times\mathbf{E}_{p-1}^{\mathrm{t}}(\mathbf{r};\cdot)=\hat{\mathbf{n}}\times\mathbf{E}_p^{\mathrm{t}}(\mathbf{r};\cdot) \tag{7}$$

$$\frac{1}{\mu_{p-1}}\hat{\mathbf{n}}\times\nabla\times\mathbf{E}_{p-1}^{\mathrm{t}}(\mathbf{r};\cdot)=\frac{1}{\mu_p}\hat{\mathbf{n}}\times\nabla\times\mathbf{E}_p^{\mathrm{t}}(\mathbf{r};\cdot) \tag{8}$$

on the boundaries of each dielectric layer V_p $(p=1,\ldots,P)$. If the core V_P is PEC or PMC, then on its boundary the following conditions hold [15]

$$\hat{\mathbf{n}}\times\mathbf{E}_{P-1}^{\mathrm{t}}(\mathbf{r};\cdot)=\mathbf{0}, \tag{9}$$

$$\hat{\mathbf{n}}\times\nabla\times\mathbf{E}_{P-1}^{\mathrm{t}}(\mathbf{r};\cdot)=\mathbf{0}. \tag{10}$$

Moreover, the total individual fields in V_0 satisfy the Silver-Müller radiation condition [16], and are expressed as

$$\mathbf{E}_0^t\left(\mathbf{r};\mathbf{r}_q^j\right)=\mathbf{g}_q^j(\hat{\mathbf{r}})h_0(k_0r)+\mathcal{O}\left(r^{-2}\right),\ r=|\mathbf{r}|\to\infty, \tag{11}$$

where $\mathbf{g}_q^j$ is the *individual far-field* due to a dipole at $\mathbf{r}_q^j\in V_q^{\mathrm{ex}}$ and h_0 is the zero-th order and first-kind spherical Hankel function. The *q-excitation* $\mathbf{g}_q$ and *overall far-field* $\mathbf{g}$ are defined as the superpositions of the individual far-fields due to all n_q dipoles in V_q^{ex} and to all N dipoles, respectively, i.e.,

$$\mathbf{g}_q(\hat{\mathbf{r}})=\sum_{j=1}^{n_q}\mathbf{g}_q^j(\hat{\mathbf{r}}), \tag{12}$$

$$\mathbf{g}(\hat{\mathbf{r}})=\sum_{q=1}^{Q}\mathbf{g}_q(\hat{\mathbf{r}}). \tag{13}$$

Next, the *individual* σ_q^j, *q-excitation* σ_q, and *overall cross section* σ are the scattering cross sections by a dipole at $\mathbf{r}_q^j\in V_q^{\mathrm{ex}}$, all dipoles in V_q^{ex}, and all N dipoles, respectively, i.e.,

$$\sigma_q^j=\frac{1}{k_0^2}\int_{S^2}\left|\mathbf{g}_q^j(\hat{\mathbf{r}})\right|^2\mathrm{d}s(\hat{\mathbf{r}}), \tag{14}$$

$$\sigma_q=\frac{1}{k_0^2}\int_{S^2}\left|\mathbf{g}_q(\hat{\mathbf{r}})\right|^2\mathrm{d}s(\hat{\mathbf{r}}), \tag{15}$$

$$\sigma=\frac{1}{k_0^2}\int_{S^2}\left|\mathbf{g}(\hat{\mathbf{r}})\right|^2\mathrm{d}s(\hat{\mathbf{r}}), \tag{16}$$

where S^2 is the unit sphere of $\mathbb{R}^3$. The overall cross section is not–in general–equal to the sum of the individual cross sections. This was elaborated in [17] for acoustic point-source excitation of a layered medium, and in [18] for acoustic plane-wave multiple scattering. For plane-wave light scattering by a small number of particles, the additivity of the cross sections was investigated in [19] under the condition of sufficiently large distance between each particle. Non-additive properties of the cross sections in conjunction with validity conditions of the Discrete Dipole Approximation (DDA) were studied in [20].

The difference between the sum of the individual cross sections and the overall cross section expresses the rate of *induced energy flux*, which stems from the interactions between the individual fields, and is not connected directly to an actual exciting dipole. This induced energy flux rate is quantified by the following *interaction scattering cross sections* (ISCS)

$$\begin{aligned}\tilde{\sigma}_q&=\sigma_q-\sum_{j=1}^{n_q}\sigma_q^j\\&=\frac{2}{k_0^2}\mathrm{Re}\left[\sum_{j=1}^{n_q-1}\sum_{\nu=j+1}^{n_q}\int_{S^2}\mathbf{g}_q^j(\hat{\mathbf{r}})\cdot\overline{\mathbf{g}_q^{\nu}(\hat{\mathbf{r}})}\mathrm{d}s(\hat{\mathbf{r}})\right],\end{aligned} \tag{17}$$

$$\sigma^{\mathrm{D}}=\sum_{q=1}^{Q}\tilde{\sigma}_q, \tag{18}$$

$$\begin{aligned}\sigma^{\mathrm{I}}&=\sigma-\sum_{q=1}^{Q}\sigma_q\\&=\frac{2}{k_0^2}\mathrm{Re}\left[\sum_{q=1}^{Q-1}\sum_{s=q+1}^{Q}\int_{S^2}\mathbf{g}_q(\hat{\mathbf{r}})\cdot\overline{\mathbf{g}_s(\hat{\mathbf{r}})}\mathrm{d}s(\hat{\mathbf{r}})\right],\end{aligned} \tag{19}$$

$$\begin{aligned}\sigma^{\mathrm{T}}&=\sigma-\sum_{q=1}^{Q}\sum_{j=1}^{n_q}\sigma_q^j\\&=\frac{2}{k_0^2}\mathrm{Re}\left[\sum_{\nu=1}^{N-1}\sum_{j=\nu+1}^{N}\int_{S^2}\mathbf{g}^{\nu}(\hat{\mathbf{r}})\cdot\overline{\mathbf{g}^j(\hat{\mathbf{r}})}\mathrm{d}s(\hat{\mathbf{r}})\right].\end{aligned} \tag{20}$$

The *q-ISCS* $\tilde{\sigma}_q$ quantifies the energy flux rate due to the interaction between the dipoles in layer V_q^{ex}. The *direct ISCS* σ^{D} is the sum of the *q-ISCS* for all Q excitation layers. The *indirect ISCS* σ^{I} accounts for the flux rate induced by the interaction between total fields generated in different excitation layers. The *total ISCS* σ^{T} quantifies the flux rate due to the interaction between all dipoles exciting the scatterer and, thus, measures all possible interactions between the participating fields. The ISCS are related by

$$\sigma^{\mathrm{T}}=\sigma^{\mathrm{D}}+\sigma^{\mathrm{I}}. \tag{21}$$

In the following sections, we present optical theorems for all cross sections involved as well as physical bounds for the ratios of the ISCS over the corresponding scattering cross sections. These theorems and physical bounds are important

in determining the additivity of the cross sections, and, moreover, elaborate that the energy flux quantified by the ISCS contributes significantly to the overall flux–especially when strong near-field interaction occurs between fields generated by the N dipoles.

III. SINGLE-LAYER EXCITATION

Single-layer excitation concerns the case of all dipoles lying in the same layer (*internal excitation*) or in the scatterer's exterior (*external excitation*); hence, it holds that $n_q = N$ and $Q = 1$. In this case, $\sigma^{\mathrm{T}} = \sigma^{\mathrm{D}} = \tilde{\sigma}_q$, $\sigma^{\mathrm{I}} = 0$, since there is no indirect interaction between the participating fields and $\sigma_q = \sigma$.

A. OPTICAL THEOREMS AND PHYSICAL BOUNDS

Using [21, Th. 5.1], we arrive at the following optical theorems relating the q-excitation cross section and the q-ISCS with their corresponding secondary fields

$$\sigma_q = 4\pi \frac{\mu_0}{k_0}\left[\sum_{j=1}^{n_q} \mathrm{Re}\left(\overline{\mathrm{i}\tilde{A}_q^j}\left(\nabla \times \mathbf{E}_q^{\mathrm{sec}}(\mathbf{r}_q^j; \mathbf{r}_q^1, \ldots, \mathbf{r}_q^{n_q})\right) \cdot \hat{\mathbf{p}}_q^j\right) + \frac{1}{2}\sum_{j=1}^{n_q}\sum_{\nu=1}^{n_q} \frac{\tilde{\sigma}_{q,j,\nu}^{\mathrm{pr}}}{k_q \mu_q}\right], \tag{22}$$

$$\tilde{\sigma}_q = 4\pi \frac{\mu_0}{k_0}\mathrm{Re}\left[\sum_{j=1}^{n_q} \overline{\mathrm{i}\tilde{A}_q^j}\left(\nabla \times \tilde{\mathbf{E}}_q^{\mathrm{sec}}(\mathbf{r}_q^j; \mathbf{r}_q^j)\right) \cdot \hat{\mathbf{p}}_q^j + \sum_{\nu=1}^{n_q-1}\sum_{j=\nu+1}^{n_q} \frac{\tilde{\sigma}_{q,j,\nu}^{\mathrm{pr}}}{k_q \mu_q}\right], \tag{23}$$

where $\tilde{A}_q^j = A_q^j/\mu_q$, while $\tilde{\mathbf{E}}_q^{\mathrm{sec}}(\mathbf{r}; \mathbf{r}_q^j)$ denotes the secondary *partial field* of V_q^{ex} with respect to a single dipole, i.e.,

$$\tilde{\mathbf{E}}_p^{\mathrm{sec}}\left(\mathbf{r}; \mathbf{r}_q^j\right) = \sum_{\substack{\nu=1 \\ \nu \neq j}}^{n_q} \mathbf{E}_p^{\mathrm{sec}}\left(\mathbf{r}; \mathbf{r}_q^\nu\right). \tag{24}$$

Quantity $\tilde{\sigma}_{q,j,\nu}^{\mathrm{pr}}$ denotes the average flux rate per surface unit area induced by the interaction of the primary far-fields generated by dipoles at $\mathbf{r}_q^j$ and $\mathbf{r}_q^\nu$ under the absence of the scatterer, and it is calculated as

$$\begin{aligned}\tilde{\sigma}_{q,j,\nu}^{\mathrm{pr}} &\equiv \frac{1}{2\pi}\int_{S^2} \overline{\mathbf{g}_{q,j}^{\mathrm{pr}}(\hat{\mathbf{r}})} \cdot \mathbf{g}_{q,\nu}^{\mathrm{pr}}(\hat{\mathbf{r}}) \mathrm{d}s(\hat{\mathbf{r}}) \\ &= A_q^\nu\left(\nabla \times \overline{\mathbf{E}^{\mathrm{pr}}\left(\mathbf{r}_q^\nu; \mathbf{r}_q^j\right)}\right) \cdot \hat{\mathbf{p}}_q^\nu \\ &\quad - \overline{A_q^j}\left(\nabla \times \mathbf{E}^{\mathrm{pr}}\left(\mathbf{r}_q^j; \mathbf{r}_q^\nu\right)\right) \cdot \hat{\mathbf{p}}_q^j.\end{aligned}$$

Employing Hölder's inequality in the definitions of the involved scattering cross sections and ISCS, we obtain the following bounds for the q-ISCS

$$1 - n_q \frac{\sigma_q^{\max}}{\sigma_q} \leq \frac{\tilde{\sigma}_q}{\sigma_q} \leq \min\left\{1 - n_q \frac{\sigma_q^{\min}}{\sigma_q}, 1 - \frac{1}{n_q}\right\}, \tag{25}$$

where $\sigma_q^{\min}$ and $\sigma_q^{\max}$ are the minimum and maximum individual cross sections for the dipoles located in V_q^{ex}. When

$$n_q^2 \sigma_q^{\min} \leq \sigma_q, \tag{26}$$

then the minimum involved in (25) is $1 - \frac{1}{n_q}$. Considering that $\sigma_q \leq n_q^2 \sigma_q^{\max}$ and combining with (25), we conclude that condition (26) holds if and only if

$$\sqrt{\frac{\sigma_q}{\sigma_q^{\max}}} \leq n_q \leq \sqrt{\frac{\sigma_q}{\sigma_q^{\min}}}. \tag{27}$$

A detailed proof of (25) is given in the Appendix. Optical theorems for a single dipole in the exterior of a homogeneous medium were established in [22]. Physical bounds for the differential radar cross sections with respect to the number of closely-spaced isotropic radiators excited by a plane wave were derived in [23].

B. PARAMETRIC ANALYSIS AND NUMERICAL RESULTS

The variations of the q-ISCS and their associated physical bounds with respect to the input parameters of the scattering problem are investigated numerically. The presented results correspond to a layered spherical scatterer V with *all* excitation dipoles lying either in the exterior of V (*external excitation*) or in a certain spherical layer (*internal excitation*). Precisely, a 2-layered spherical scatterer V (i.e., $P = 2$) is considered with external radius a_1 and core's radius a_2, excited by external dipoles in V_0 ($r > a_1$) or internal dipoles in the spherical shell V_1 ($a_2 < r < a_1$). The core V_2 ($0 \leq r < a_2$) is PEC or dielectric.

Concerning the choices of physical parameters and thicknesses of the shells, connections can be established to potential applications, among the ones identified in the Introduction above. For example, in applications involving biological tissues, the magnetic permeability is considered to be that of vacuum, and hence the relative permeability is $\mu_r = 1$ [9], [11]. However, the relative dielectric permittivities of biological tissues depends on many factors, including excitation frequency, e.g., the dielectric permittivity of human lung tissue is 2.2 at 1 GHz [27]. On the other hand, in hyperthermia techniques, a multi-slot coaxial antenna, with central conductor's (core's) radius less than 1/5 of the antenna (catheter) radius is frequently employed [3], [4]. Besides, in the spherical three-shell model of the brain, the brain's (core's) radius is at least half the head's external radius [2].

The associated boundary-value problems are solved by employing the methodology developed in [24]–[26], which combines the Sommerfeld's and T-matrix methods in conjunction with suitable eigenfunction expansions. This methodology is entirely analytical and does not require any restrictions on the problem's parameters. Moreover, its validity was tested with respect to other solutions having appeared in the literature as well as to special cases of the considered spherical geometry and involved materials (see [24, Secs. 5 and 6] and [25, Secs. 4 and 6]).

TABLE 1. Scattering cross sections corresponding to the external excitation of a homogeneous dielectric spherical scatterer by $N = 4$ external dipoles for different relative dielectric permittivities ϵ_{r1} and radii $k_0 a_1$.

$k_0 a_1 = 0.1$					
	$\epsilon_{r1} = 2$	$\epsilon_{r1} = 5$	$\epsilon_{r1} = 10$	$\epsilon_{r1} = 25$	$\epsilon_{r1} = 50$
σ_0^1	0.0011	0.0057	0.0098	0.0139	0.0159
σ_0^2	0.0008	0.0040	0.0069	0.0097	0.0110
σ_0^3	0.0006	0.0029	0.0051	0.0072	0.0081
σ_0^4	0.0004	0.0023	0.0039	0.0055	0.0063
σ^{T}	0.0082	0.0429	0.0742	0.1047	0.1189
σ	0.0110	0.0578	0.0999	0.1410	0.1602
$k_0 a_1 = 2.5$					
	$\epsilon_{r1} = 2$	$\epsilon_{r1} = 5$	$\epsilon_{r1} = 10$	$\epsilon_{r1} = 25$	$\epsilon_{r1} = 50$
σ_0^1	1.9329	3.5090	17.3278	1.0508	2.6877
σ_0^2	1.8850	3.1956	10.5819	0.9309	2.5625
σ_0^3	1.8639	3.1722	8.3120	0.8994	2.5140
σ_0^4	1.8528	3.1984	7.3297	0.8906	2.4912
σ^{T}	22.2841	34.7086	102.3401	10.2054	29.8567
σ	29.8188	47.7837	145.8915	13.9771	40.1121
$k_0 a_1 = 10$					
	$\epsilon_{r1} = 2$	$\epsilon_{r1} = 5$	$\epsilon_{r1} = 10$	$\epsilon_{r1} = 25$	$\epsilon_{r1} = 50$
σ_0^1	1.9653	2.6764	3.2267	3.2713	2.2136
σ_0^2	1.8769	2.6713	2.7717	3.0155	2.1135
σ_0^3	1.8618	2.6919	2.6491	2.9365	2.0930
σ_0^4	1.8595	2.7091	2.5974	2.9016	2.0863
σ^{T}	14.5786	24.4082	20.5329	26.3146	19.4578
σ	22.1421	35.1568	31.7778	38.4395	27.9642

First, we consider the external excitation of a homogeneous dielectric spherical scatterer by $N = 4$ dipoles lying on the z-axis at $r_j = (1 + 0.25j)a_1$, for $j = 1, 2, 3, 4$. For the scatterer's dielectric permittivity ϵ_{r1} different values are examined, while its relative magnetic permeability is $\mu_{r1} = 1$. Table 1 presents the values of the individual cross sections σ_0^j, the total ISCS σ^{T}, and the overall cross section σ for different ϵ_{r1} and electric radii $k_0 a_1$. For the computation of the individual cross sections, we used the exact solution of the direct scattering problem due to a single source developed in [24]. For the overall cross section and the total ISCS, we used the optical theorems (22) and (23). From this table, it is readily observed that $\sigma = \sigma^{\mathrm{T}} + \sum_{j=1}^{4} \sigma_0^j$ for all depicted cases.

Then, in Fig. 2, we depict the variations of $\sigma^{\mathrm{T}}/\sigma$ versus the electric radius $k_0 a_1$ for a group of $N = 4$ external dipoles lying in close proximity, but at different distances from the scatterer's boundary, precisely at: $r_j = (1.3 + 0.2j)a_1$, $r_j = (2.3 + 0.2j)a_1$, and $r_j = (3.3 + 0.2j)a_1$, with $j = 0, 1, 2, 3$. The ISCS ratios are oscillatory for higher frequencies when the dipoles lie close to the sphere, but, still they remain within a 4% and a 5% range in the PEC and dielectric core case, respectively. As the group of dipoles moves away from the sphere, an oscillatory behavior remains, but the variation range is very small, so that we can safely assume that the ISCS ratios are equal for all examined frequencies to the upper bound $1 - \frac{1}{N} = 0.75$ of (25).

Similar conclusions are drawn from Fig. 3, in which the distance between successive dipoles is taken to be half the

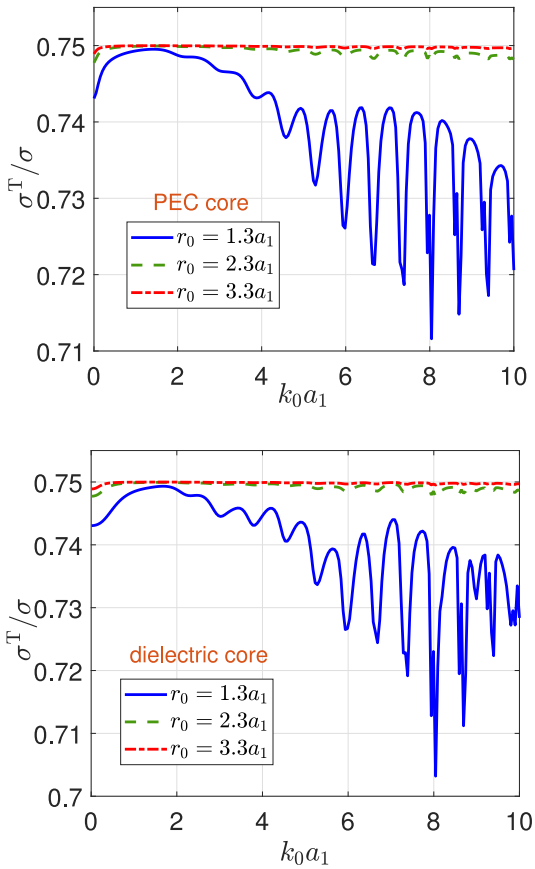

FIGURE 2. ISCS ratios $\sigma^{\mathrm{T}}/\sigma$ versus $k_0 a_1$ for a spherical scatterer with $a_1 = 2a_2$, $\epsilon_{r1} = 2$, $\mu_{r1} = 1.5$ and a PEC core (top panel) and dielectric core with $\epsilon_{r2} = 3$, $\mu_{r2} = 2.5$ (bottom panel). The scatterer is excited by three sets of $N = 4$ external sources with distance $0.2a_1$ between successive sources.

sphere's radius, namely $r_j = (1.3 + 0.5j)a_1$, $r_j = (2.3 + 0.5j)a_1$, and $r_j = (3.3 + 0.5j)a_1$ with $j = 0, 1, 2, 3$. The only notable difference is that in this case, the variations of $\sigma^{\mathrm{T}}/\sigma$, when the dipoles lie close to the sphere, are larger with the ranges being 17% for the PEC and 20% for the dielectric core.

In Fig. 4, we depict the ISCS ratios and the physical bounds indicated by (25) for external excitation by $N = 4$ dipoles at $r_j = (1.25 + 0.25j)a_1$, with $j = 0, 1, 2, 3$. In the lower frequencies ($k_0 a_1 < 3.1$ for the PEC and $k_0 a_1 < 2.1$ for the dielectric core), the upper bound of (25) is $1 - 1/N$, which implies that in these regions holds $\sigma_q^{\min} \leq \sigma/N^2$. Furthermore, we observe that for all examined frequencies and both types of cores the differences between the upper bound and the actual ISCS ratio are less than 1%. On the other hand, the differences between the lower and the upper bounds of (25) are less than 4% for $k_0 a_1 \geq 1$. In the insets, we show the variations of the ISCS ratios in the low-frequency region, in particular for $k_0 a_1 \leq 1$. In this region, the q-interaction ISCS ratios are much closer to the upper than to the lower bounds of (25). This is due to the fact that the ratios of the minimum and maximum cross sections over the q-excitation cross section differ substantially. Precisely, for $k_0 a_1 \leq 0.5$, their differences can exceed 5%,

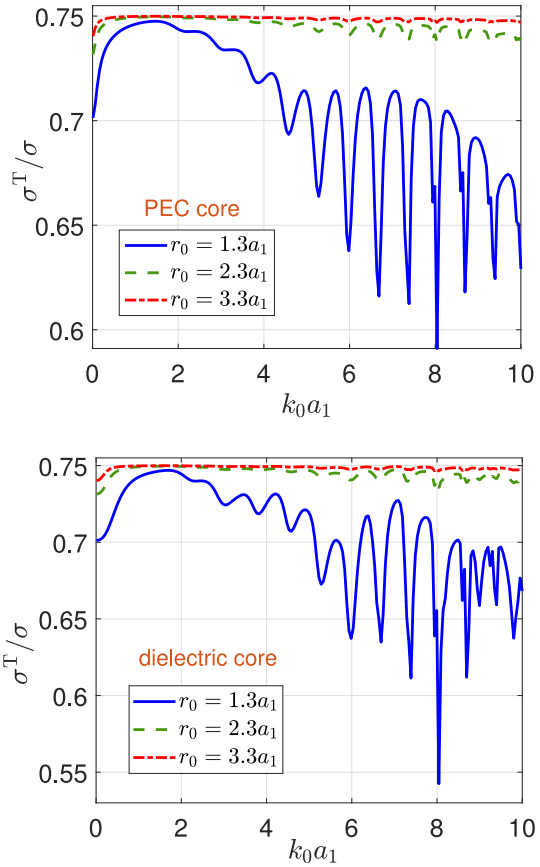

FIGURE 3. As in Fig. 2, but for distance $0.5a_1$ between successive sources.

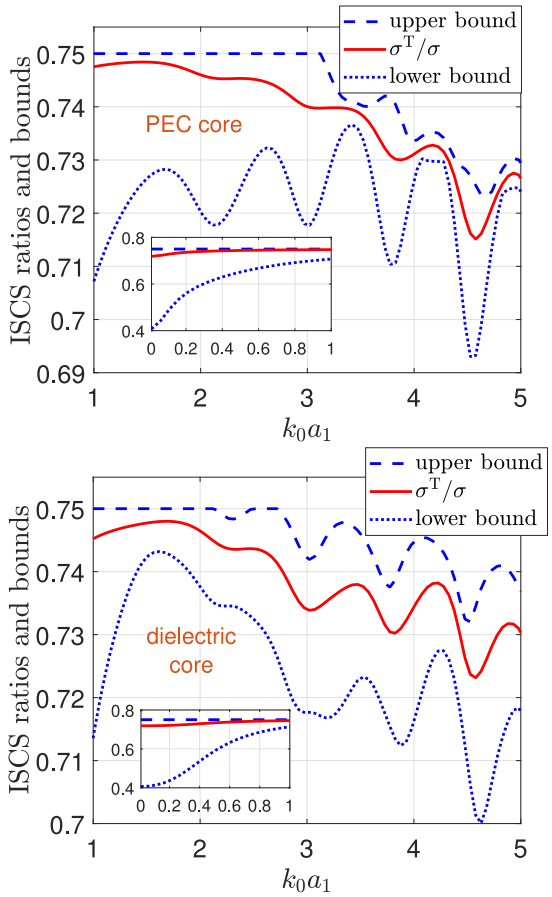

FIGURE 4. ISCS ratios $\sigma^{\mathrm{T}}/\sigma$ and their physical bounds versus k_0a_1 of a 2-layered sphere with $a_1 = 2a_2$, $\epsilon_{r1} = 2$, $\mu_{r1} = 1.5$ and a PEC core (top panel) or a dielectric core (bottom panel) with $\epsilon_{r2} = 3$ and $\mu_{r2} = 2.5$. The scatterer is excited by $N = 4$ external dipoles.

which yields at least a 20% difference between the physical bounds.

The ISCS ratios and associated physical bounds from (25) are shown in Fig. 5 for the case of $N = 4$ internal dipoles located at $r_j = (0.65+0.05j)a_1$, with $j = 0, 1, 2, 3$. A steeper descent of the q-excitation ISCS ratio is now observed compared to the external excitation case of Fig. 4. For lower frequencies ($k_0a_1 < 3.5$ for the PEC and $k_0a_1 < 2.5$ for the dielectric core), the upper bound of (25) is $1-1/N$. The differences between the lower and the upper bounds of (25) are larger compared to the corresponding differences for external excitation; in some cases they now reach 15%. In the low-frequency region (i.e., $k_0a_1 \leq 1$), the ISCS ratio almost coincides to its upper bound. Another difference between the behavior of the ISCS ratios for external and internal excitation is that in external excitation, for the frequencies where $\sigma^{\min} \geq \sigma/N^2$, all quantities show a uniform behavior, while in internal excitation, the ISCS ratios seem to act as a "mirror" between the lower and upper bounds.

Figure 6 depicts the physical bounds for the number N of dipoles that excite the spherical scatterer. All dipoles are external and lie at $r_1 = 2.5a_1, r_2 = 2.8a_1, r_3 = 3.1a_1, r_4 = 3.5a_1$. We observe the almost identical behavior of the physical bounds for both cores, especially in the higher frequencies. Some slight differences occur in the lower frequencies. In particular, for $0.2 < k_0a_1 < 1.5$ for the dielectric core and for $0.1 < k_0a_1 < 2.5$ for the PEC core, we see that the physical bounds are valid and determine accurately the number of dipoles exciting the scatterer. For $k_0a_1 < 0.2$, for the dielectric core, and for $k_0a_1 < 0.1$, for the PEC core, the physical bounds remain valid, but they cannot be used to accurately determine the number of dipoles; this is explained by the significant difference between the minimum and maximum individual cross sections in the low-frequency region. However, for $k_0a_1 > 1.5$, for the dielectric core, and for $k_0a_1 > 2.5$, for the PEC core, where the minimum and maximum individual cross sections are very close, we observe that it holds $N = [\sqrt{\sigma/\sigma^{\min}}] + 1$, where $[x]$ denotes the integer part of x. We note, that even sparser or denser dipole distributions have been found to exhibit similar patterns with respect to the physical bounds.

In Fig. 7, we depict the variations of $\sigma^{\mathrm{T}}/\sigma$ versus the relative permittivity ϵ_{r1} of the first spherical shell, for a scatterer with PEC or dielectric core, excited by $N = 4$ external dipoles located at $r_1 = 1.3a_1, r_2 = 1.8a_1, r_3 = 2.3a_1, r_4 = 2.8a_1$ on the z-axis. For the higher frequency, $\sigma^{\mathrm{T}}/\sigma$ change only slightly with ϵ_{r1}, i.e., less than 2% for the PEC core and less than 3% for the dielectric core. Furthermore, for both types of cores, $\sigma^{\mathrm{T}}/\sigma$ decreases in an oscillating manner with increasing ϵ_{r1}. For the lower frequency, the behavior is

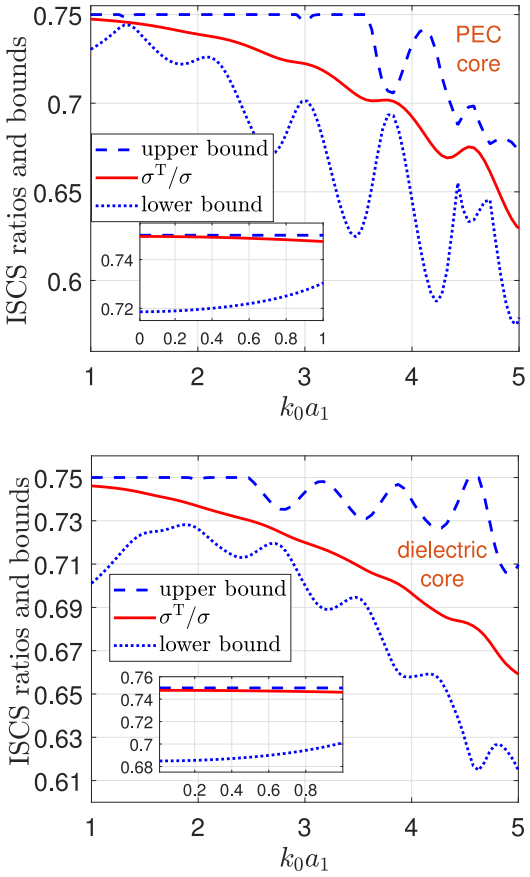

FIGURE 5. As in Fig. 4, but for excitation due to $N = 4$ internal dipoles.

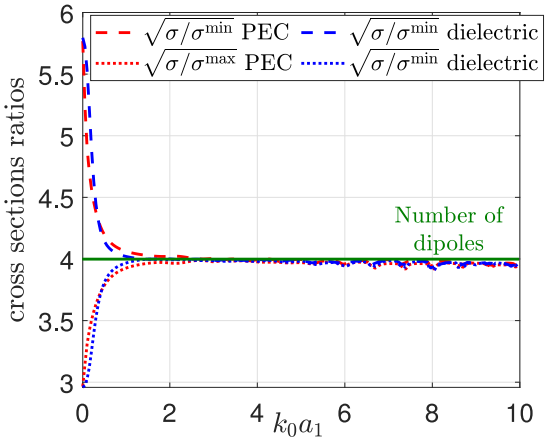

FIGURE 6. Physical bounds for the number N of dipoles exciting a 2-layered sphere with $a_1 = 2a_2$, $\epsilon_{r1} = 2$, $\mu_{r1} = 1.5$. The bounds for a PEC core are depicted with red and the bounds for a dielectric core with blue color. For the dielectric core, its parameters are $\epsilon_{r2} = 3$ and $\mu_{r2} = 2.5$. The scatterer is excited by $N = 4$ dipoles, all of them lying in the exterior of the sphere.

different: σ^T/σ increases with ϵ_{r1} and then stabilizes when $\epsilon_{r1} = 2$ for the PEC and $\epsilon_{r1} = 3$ for the dielectric core. The ranges of σ^T/σ are less than 2% and 8% for the PEC and dielectric core, respectively.

In Fig. 8, we show the variations of σ^T/σ for $N = 4$ dipoles located on the z-axis and in the first shell V_1 of a sphere V with a PEC core V_2 of radius $a_2 = a_1/5$. The

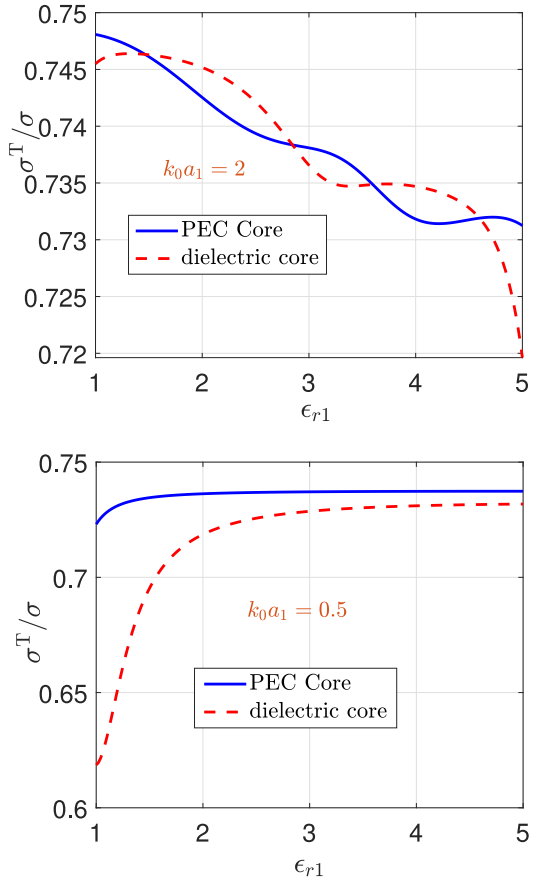

FIGURE 7. ISCS ratios σ^T/σ versus the relative permittivity ϵ_{r1} of a 2-layered spherical scatterer with $a_1 = 2a_2$, $\mu_{r1} = 1.5$ and $k_0a_1 = 2$ (top panel) or $k_0a_1 = 0.5$ (bottom panel) with $\epsilon_{r1} = 1.5\epsilon_2$ and $\mu_{r2} = 2.5$. The scatterer is excited by $N = 4$ external dipoles.

following three dipoles distributions are considered: "core side" where the dipoles are located closer to the core V_2, "middle side" where the dipoles are in the middle of V_1, and "boundary side" where the dipoles are closer to the boundary of V. In the top panel, the distance between successive dipoles is $0.05a_1$, while in the bottom panel the corresponding distance is $0.1a_1$. We notice that for $k_0a_1 \leq 5$ the ISCS ratios are smooth and descending for all distributions. For $k_0a_1 \geq 5$, oscillations appear for the distributions away from the core, but not for the distribution closer to the core. For the denser distribution, not so significant changes occur in the ISCS ratios with respect to the placement of the dipoles. The situation is different for the less dense distribution, where for higher frequencies rapid oscillations occur for the distribution closer to the scatterer's boundary. Particularly, for $k_0a_1 \geq 7$, the ISCS ratios obtain also negative values, which implies the reduction of the energy flux rate. The ranges of the ISCS ratios are smaller for the dense dipoles (less than 35%) and larger for the less dense dipoles (more than 120%). A sparser dipole distribution will lead to an even less-predictable ISCS ratios' behavior.

Figure 9 depicts the variations of the ISCS values for the same distributions of Fig. 8. We see that the values follow a somewhat different pattern than the ratios. Dense

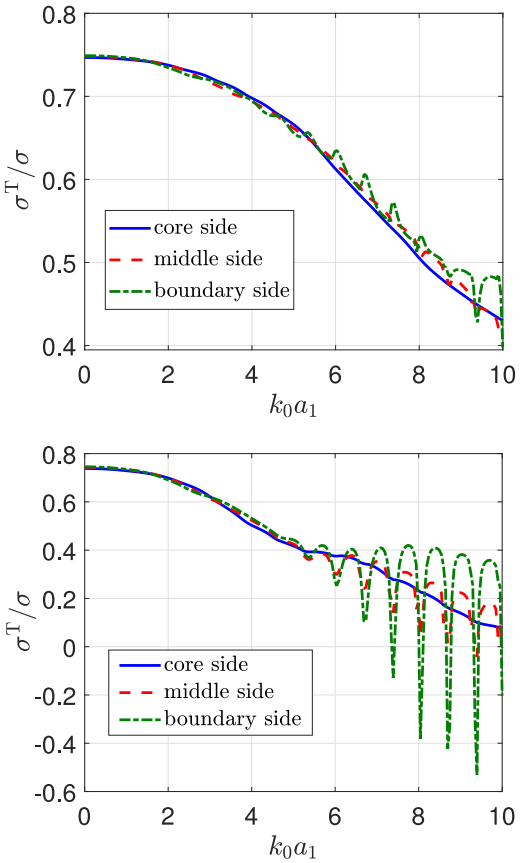

FIGURE 8. ISCS ratios $\sigma^{\mathrm{T}}/\sigma$ for $N = 4$ dipoles lying in the first shell of a 2-layered sphere with $\mu_{r1} = 1.5$, $\epsilon_{r1} = 2$ and PEC core of radius $a_2 = a_1/5$. Top panel: dense dipole distribution with $r_1^{j+1} - r_1^j = 0.05a_1$ $(j = 1, 2, 3)$ and $r_1^1 = 0.25a_1$ (core), $r_1^1 = 0.55a_1$ (middle), $r_1^1 = 0.8a_1$ (boundary side). Bottom panel: a less dense dipole distribution with $r_1^{j+1} - r_1^j = 0.1a_1$ $(j = 1, 2, 3)$ and $r_1^1 = 0.25a_1$ (core), $r_1^1 = 0.45a_1$ (middle), $r_1^1 = 0.65a_1$ (boundary side).

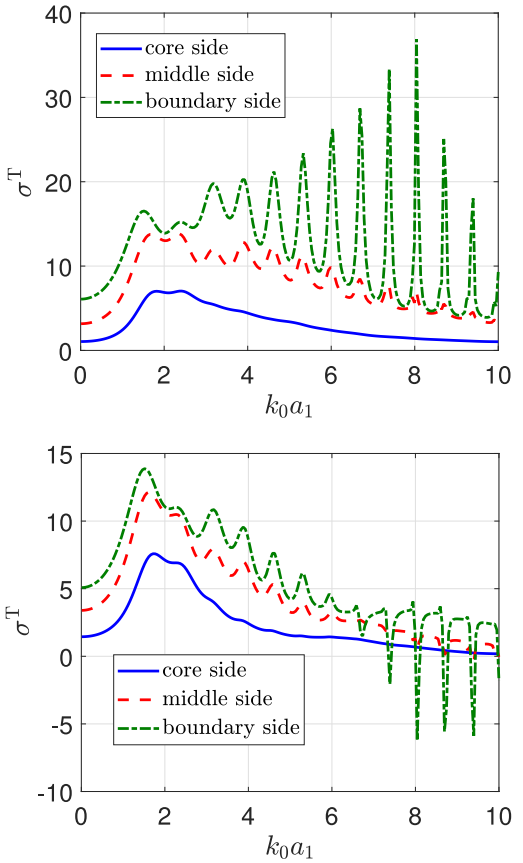

FIGURE 9. Total ISCS σ^{T} values for the same setup of Fig. 8.

distributions show large ISCS ranges, but small ranges in the corresponding ratios (as we have seen above). For dipoles groups nearer the sphere's core, the ISCS values decrease and approach zero in higher frequencies. Less dense distributions show significantly smaller ISCS values, and negative values in higher frequencies. Besides, when the dipoles are closer to the sphere's core, the differences in the ISCS values between dense and less dense distributions are small.

In Fig. 10, we depict the overall cross section σ and total ISCS ratio $\sigma^{\mathrm{T}}/\sigma$ versus the radius k_0a_1 in case of a sphere with dielectric core of different radii a_2 excited by $N = 4$ internal sources in shell V_1. For all the examined core's radii, the values of σ remain fairly the same and oscillate rapidly (after $k_0a_1 > 1.2$); the latter is expected from the discussions of [21], [26]. The ratios $\sigma^{\mathrm{T}}/\sigma$ descent smoothly for $k_0a_1 < 5$, oscillate rapidly for $k_0a_1 > 5$, and are not significantly affected by changes in the core's radii.

Figure 11 shows the overall cross section σ and total ISCS σ^{T} at the fixed frequency $k_0a_1 = 1$ for a spherical scatterer with a PEC core. We consider the cross sections variations as one, two, and three dipoles move from their original positions at a distance R (the moving dipoles are each time the ones being further away from the scatterer). In particular, the initial positions are $r_j = (1.3+0.2j)$ with $j = 0, 1, 2, 3$, while the moving dipoles' locations are given by $r_j(R) = r_jR$ with $j = 1, 2, 3$. A notable similarity is observed in these figures since both σ and σ^{T} follow a similar pattern: they decrease as more dipoles move further away from their original to a sparser distribution. This fact indicates that the ratio $\sigma^{\mathrm{T}}/\sigma$ remains fairly unchanged. The ranges of σ and σ^{T} increase with the number of moving dipoles. The above conclusions have been found to be similar for the dielectric core (not shown here) with the only difference that the ranges of σ and σ^{T} are much smaller than for the PEC core.

IV. MIXED EXCITATION

Mixed excitation refers to the case of dipoles located in more than one excitation layers. Then, the indirect ISCS σ^{I} is–in general–non zero.

A. OPTICAL THEOREMS AND PHYSICAL BOUNDS

First, we provide two optical theorems relating the overall cross section and the indirect ISCS with the corresponding secondary fields

$$\sigma = \frac{4\pi\mu_0}{k_0}\left[\mathrm{Re}\left(\sum_{q=1}^{Q}\sum_{j=1}^{n_q}\overline{\mathrm{i}\tilde{A}_q^j}\left(\nabla\times\mathbf{E}_q^{\mathrm{sec}}(\mathbf{r}_q^j;\mathbf{r}^1,\ldots,\mathbf{r}^N)\right)\cdot\hat{\mathbf{p}}_q^j\right) + \frac{1}{2}\sum_{q=1}^{Q}\sum_{j=1}^{n_q}\sum_{\nu=1}^{n_q}\frac{\tilde{\sigma}_{q,j,\nu}^{\mathrm{pr}}}{k_q\mu_q}\right], \tag{28}$$

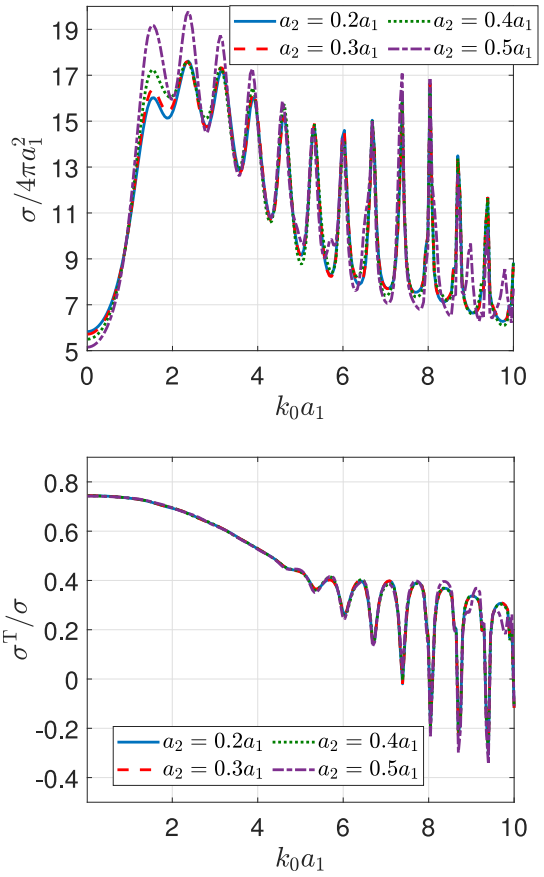

FIGURE 10. Overall cross section σ (top panel) and total ISCS ratios $\sigma^{\mathrm{T}}/\sigma$ (bottom panel) versus the radius $k_0 a_1$ for $\epsilon_{r1} = 2$, $\epsilon_{r2} = 3$, $\mu_{r1} = 1.5$, $\mu_{r2} = 2.5$, and $N = 4$ internal sources at $r_1^1 = 0.6a_1$, $r_1^2 = 0.7a_1$, $r_1^3 = 0.8a_1$, $r_1^4 = 0.9a_1$. Different radii of the dielectric core are considered.

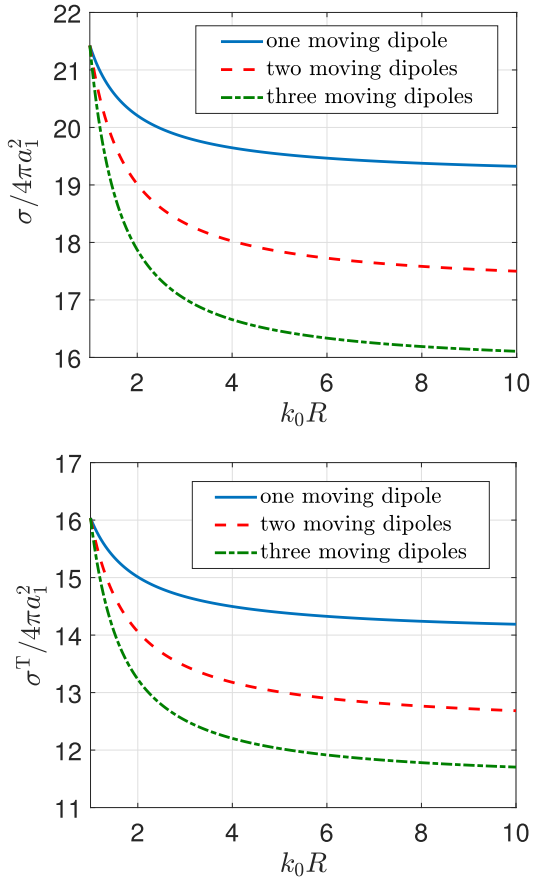

FIGURE 11. Overall cross section σ (top panel) and total ISCS σ^{T} (bottom panel) of a 2-layered scatterer with $k_0 a_1 = 1$, $\epsilon_{r1} = 2$, $\mu_{r1} = 1.5$ and a PEC core, excited by $N = 4$ sources at $r_0^1 = 1.3a_1$, $r_0^2 = 1.5a_1$, $r_0^3 = 1.7a_1$, $r_0^4 = 1.9a_1$, as a number of dipoles (one, two and three) move away from the original position by a distance R.

$$\sigma^{\mathrm{I}}(\hat{\mathbf{r}}) = \frac{4\pi\mu_0}{k_0} \times \mathrm{Re}\left(\sum_{q=1}^{Q}\sum_{j=1}^{n_q} \overline{\mathrm{i}\tilde{A}_q^j}\left(\nabla \times \tilde{\mathbf{E}}_q^{\mathrm{sec}}\left(\mathbf{r}_q^j; \mathbf{r}_q^1, \ldots, \mathbf{r}_q^{n_q}\right)\right) \cdot \hat{\mathbf{p}}_q^j\right), \tag{29}$$

where

$$\tilde{\mathbf{E}}_p^{\mathrm{sec}}\left(\mathbf{r}; \mathbf{r}_q^1, \ldots, \mathbf{r}_q^{n_q}\right) = \sum_{\substack{s=1 \\ s\neq q}}^{Q} \mathbf{E}_p^{\mathrm{sec}}\left(\mathbf{r}; \mathbf{r}_s^1, \ldots, \mathbf{r}_s^{n_s}\right) \tag{30}$$

is the *q-partial field* with respect to excitation layer V_q^{ex}, i.e., the sum of all q-excitation fields except those due to the dipoles of V_q^{ex}. Combining (21), (23), and (29) an optical theorem for the total ISCS σ^{T} can be also obtained.

Radiation from the primary fields does not appear in (29), since all interactions between primary fields are included in the direct ISCS σ^{D}. Indirect ISCS σ^{I} is, in fact, a measure of the energy flux rate due to interactions of secondary fields induced by dipoles within different layers.

The following physical bounds for σ^{I} and σ^{T} are derived

$$1 - Q\frac{\sigma_{\mathrm{ex}}^{\max}}{\sigma} \leq \frac{\sigma^{\mathrm{I}}}{\sigma} \leq \min\left\{1 - Q\frac{\sigma_{\mathrm{ex}}^{\min}}{\sigma}, 1 - \frac{1}{Q}\right\}, \tag{31}$$

$$1 - N\frac{\sigma^{\max}}{\sigma} \leq \frac{\sigma^{\mathrm{T}}}{\sigma} \leq \min\left\{1 - N\frac{\sigma^{\min}}{\sigma}, 1 - \frac{1}{N}\right\}, \tag{32}$$

where $\sigma_{\mathrm{ex}}^{\min}$ and $\sigma_{\mathrm{ex}}^{\max}$ are the minimum and maximum q-excitation cross sections and $\sigma^{\min}$ and $\sigma^{\max}$ are the minimum and maximum individual cross sections of all dipoles. We note that (25) holds in the mixed excitation case as well. For the proofs of (31) and (32), we refer to the Appendix. When

$$Q^2\sigma_{\mathrm{ex}}^{\min} \leq \sigma \tag{33}$$

$$N^2\sigma^{\min} \leq \sigma \tag{34}$$

then the minima involved in (31), (32) are $1 - \frac{1}{Q}$ and $1 - \frac{1}{N}$, respectively. Taking into account that $\sigma \leq Q^2\sigma_{\mathrm{ex}}^{\max}$ and $\sigma \leq N^2\sigma^{\max}$, and combining with (31), (32), we conclude that conditions (33), (34) hold respectively, if and only if

$$\sqrt{\frac{\sigma}{\sigma_{\mathrm{ex}}^{\max}}} \leq Q \leq \sqrt{\frac{\sigma}{\sigma_{\mathrm{ex}}^{\min}}}, \tag{35}$$

$$\sqrt{\frac{\sigma}{\sigma^{\max}}} \leq N \leq \sqrt{\frac{\sigma}{\sigma^{\min}}}. \tag{36}$$

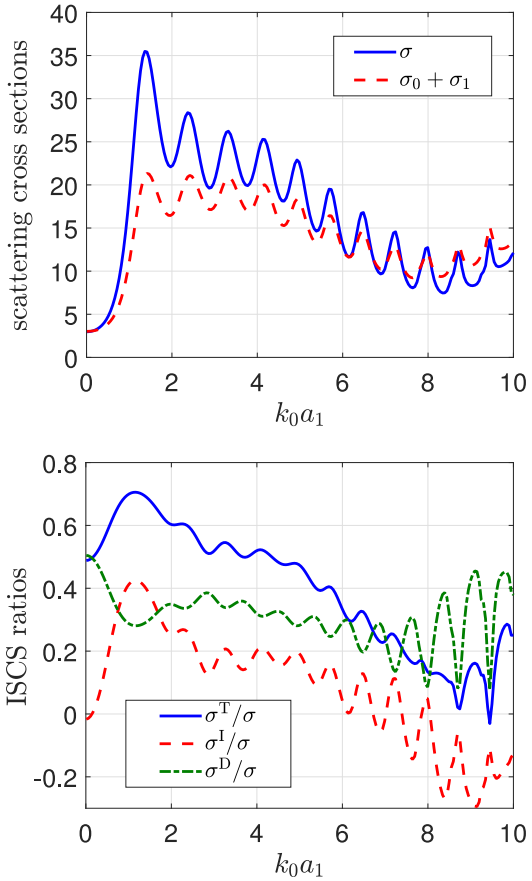

FIGURE 12. Overall cross section, 0-excitation and 1-excitation cross sections (top panel) and ISCS ratios (bottom panel) versus radius $k_0 a_1$ of a 2-layered sphere V with $\epsilon_{r1} = 2$, $\mu_{r1} = 1.25$ and a PEC core excited by $N = 4$ dipoles; $n_1 = 2$ dipoles lie in the exterior of V at $r_0^1 = 1.3a_1$, $r_0^2 = 1.8a_1$, and $n_2 = 2$ in the first shell of V at $r_1^1 = 0.7a_1$, $r_2^1 = 0.9a_1$.

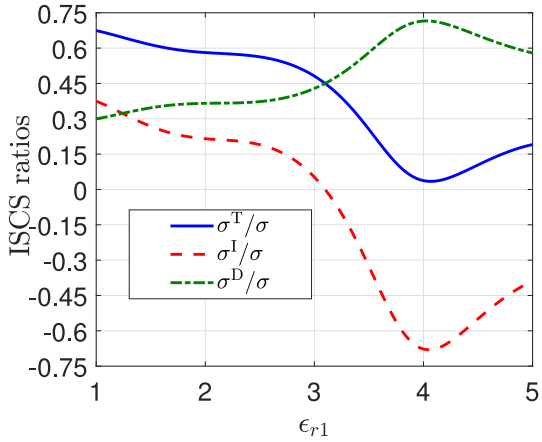

FIGURE 13. Total $\sigma^{\mathrm{T}}/\sigma$, indirect $\sigma^{\mathrm{I}}/\sigma$ and direct $\sigma^{\mathrm{D}}/\sigma$ ISCS ratios versus the relative permittivity ϵ_{r1} of a 2-layered scatterer with $k_0 a_1 = 2$, $\mu_{r1} = 1.5$, and a PEC core, excited by $N = 4$ dipoles; two lie in the exterior of the sphere at $r_0^1 = 1.3a_1$, $r_0^2 = 1.8a_1$ and two in the first shell at $r_1^1 = 0.7a_1$, $r_1^2 = 0.9a_1$.

Scattering relations and optical theorems for a layered magneto-dielectric medium excited by two internal or external dipoles and a layered acoustic medium excited by N internal or external point sources were derived in [21] and [17], respectively.

B. PARAMETRIC ANALYSIS AND NUMERICAL RESULTS

Now, we consider that the scatterer V is excited by two dipoles in the external region V_0 ($r > a_1$) and two dipoles in the first spherical shell V_1 ($a_2 < r < a_1$); hence we have $Q = 2$ excitation layers.

In Fig. 12, we depict the overall cross section σ and the sum of 0-excitation σ_0 and 1-excitation σ_1 cross sections as well as the total $\sigma^{\mathrm{T}}/\sigma$, indirect $\sigma^{\mathrm{I}}/\sigma$, and direct $\sigma^{\mathrm{D}}/\sigma$ ISCS ratios. We observe that σ gradually converges to the sum $\sigma_0 + \sigma_1$, and that $\sigma_0 + \sigma_1 > \sigma$ for $k_0 a_1 > 8$. This is explained from the behavior of the ISCS ratios, where, for $k_0 a_1 > 8$, we see that $\sigma^{\mathrm{I}}/\sigma < 0$, which in turn means that $\sigma^{\mathrm{I}} < 0$. In particular, it holds $\sigma = \sigma_0 + \sigma_1 + \sigma^{\mathrm{I}}$; see (19). Hence, larger ratios $\sigma^{\mathrm{I}}/\sigma$ lead to larger differences between the sum of q-excitation and the overall cross sections.

Figure 13 shows the variations of the total $\sigma^{\mathrm{T}}/\sigma$, the indirect $\sigma^{\mathrm{I}}/\sigma$, and the direct $\sigma^{\mathrm{D}}/\sigma$ ISCS ratios versus the relative dielectric permittivity ϵ_{r1} of a 2-layered sphere with $k_0 a_1 = 2$ and a PEC core. The ratio $\sigma^{\mathrm{I}}/\sigma$, and hence the indirect ISCS σ^{I}, becomes negative for $\epsilon_{r1} > 3.1$. For $\epsilon_{r1} = 4$, ratios $\sigma^{\mathrm{T}}/\sigma$ and $\sigma^{\mathrm{I}}/\sigma$ are minimized, while the direct $\sigma^{\mathrm{D}}/\sigma$ ISCS ratio (the sum of the 0- and 1-ISCS) is maximized; see (18). Corresponding results for the variations of the ISCS with respect to the magnetic permeability μ_{r1} have been also derived and the conclusions are the same with the ones drawn above with the only difference being that the range of ISCS variations is now smaller.

In Fig. 14, we depict the physical bounds for the number Q of excitation layers indicated by (35). The considered number $Q = 2$ is depicted with a straight red line. For $k_0 a_1 > 1$, the physical bounds can be used to determine Q for a wide range of the examined frequencies. The upper physical bound for $k_0 a_1 > 1$ remains very close to the number Q of excitation layers even when the upper bound is not valid. In fact, we see that $Q = [\sqrt{\sigma/\sigma_{\mathrm{ex}}^{\max}}] + 1$. The insets demonstrate the variations in the low-frequency region. For the PEC core, the bounds remain valid, but for $k_0 a_1 \leq 0.5$ cannot be safely used for the determination of Q, since the minimum q-excitation cross section–σ_1 in this case–is significantly smaller than the overall cross section. For the dielectric core, the physical bounds remain valid for $k_0 a_1 < 0.7$. Besides, for both types of cores a change in the minimum and maximum q-excitation cross sections occurs at $k_0 a_1 = 1$. Precisely, for $k_0 a_1 < 1$ it holds $\sigma_0 < \sigma_1$, while for $k_0 a_1 > 1$ it holds $\sigma_0 > \sigma_1$.

Figure 15 depicts the variations of $\sigma^{\mathrm{T}}/\sigma$ and $\sigma^{\mathrm{I}}/\sigma$ for $k_0 a_1 = 1$ and $k_0 a_1 = 2.5$ versus the distance $k_0 R$ between the internal group of $n_1 = 2$ dipoles, initially located at $r_1^1 = 0.8a_1$, $r_1^2 = 0.9a_1$, and the external group of $n_0 = 2$ dipoles, initially located at $r_0^1 = 1.2a_1$, $r_0^2 = 1.3a_1$. In the top panel, the internal group moves towards the sphere's core and the external group moves away from the scatterer's boundary with increasing R. Precisely, the moving dipoles' locations are given by $r_0^j(R) = r_0^j R$ for the external group

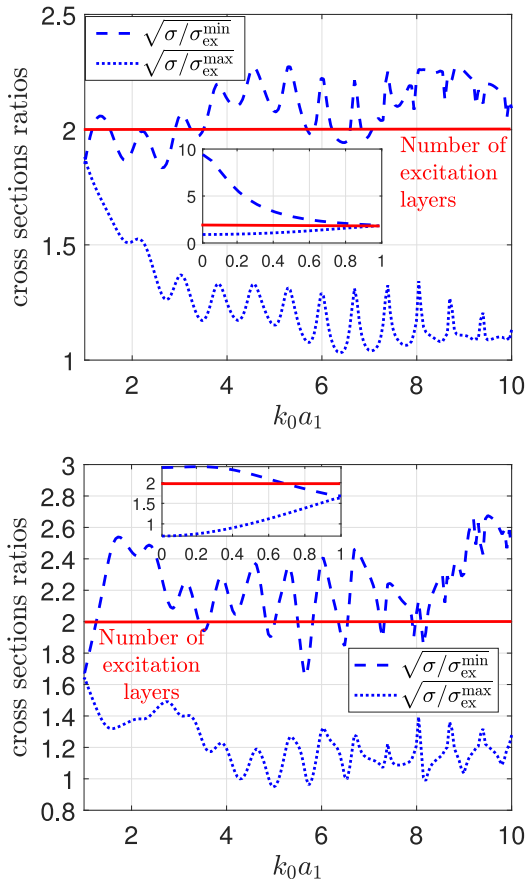

FIGURE 14. Physical bounds for the number Q of excitation layers versus k_0a_1 of a 2-layered sphere with $a_1 = 2a_2$, $\epsilon_{r1} = 2$, $\mu_{r1} = 1.5$ and a PEC core (top panel) or a dielectric core (bottom panel) with $\epsilon_{r2} = 3$ and $\mu_{r2} = 2.5$. The scatterer is excited by $N = 4$ dipoles, two lying in the exterior of the sphere and two in the first spherical shell.

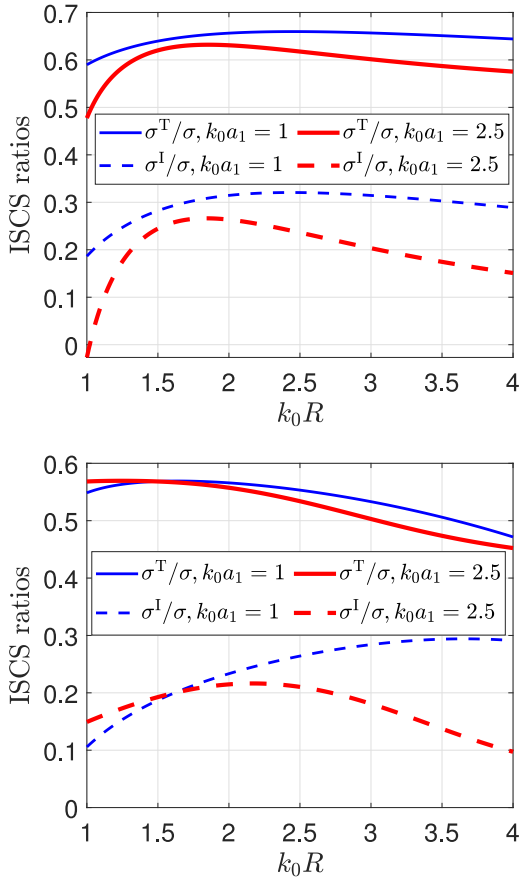

FIGURE 15. Total $\sigma^{\rm T}/\sigma$ and indirect $\sigma^{\rm I}/\sigma$ ISCS ratios versus the dipoles distance k_0R for $k_0a_1 = 1$ and k_0a_1=2.5 for a 2-layered scatterer with a dielectric core and parameters $\mu_{r1} = 1.5$, $\mu_{r2} = 2.5$, $\epsilon_{r1} = 2$, $\epsilon_{r2} = 3$, $a_2 = a_1/10$. The sphere is excited by $N = 4$ dipoles; two external and two in the first shell, at varying positions.

and $r_1^j(R) = r_1^j/R$ for the internal group. The initial setup (before moving the dipoles) corresponds to a negative $\sigma^{\rm I}/\sigma$. We observe that for both frequencies the ISCS ratios $\sigma^{\rm T}/\sigma$ and $\sigma^{\rm I}/\sigma$ follow a similar pattern: they first increase until a certain value of k_0R and then decrease. For the lower frequency, the variations of the ISCS ratios are smaller. In the bottom panel, the meaning of R is slightly different: the initial locations are $r_1^1 = 0.21a_1$, $r_1^2 = 0.2475a_1$ for the internal group and $r_0^1 = 1.2a_1$, $r_0^2 = 1.3a_1$ for the external group. The dipoles located at $r_1^1 = 0.21a_1, r_0^1 = 1.2a_1$ remain fixed, while the one at $r_1^2 = 0.2475a_1$ moves towards the scatterer's boundary, and the one at $r_0^2 = 1.3a_1$ moves away from it. The moving dipoles' locations are given by $r_q^2(R) = r_q^2R$ for $q = 0, 1$. The behavior of the ISCS is different now: for the lower frequency, we see a steeper decrease in $\sigma^{\rm T}/\sigma$ and a sharper increase in $\sigma^{\rm I}/\sigma$. Thus, the direct ISCS will decrease more rapidly than the total ISCS. Furthermore, a crossover is observed at $k_0R = 1.6$ between $\sigma^{\rm T}/\sigma$ and $\sigma^{\rm I}/\sigma$ for the two examined frequencies. This is due to that the decrease in $\sigma^{\rm T}/\sigma$ is steeper for the higher than the lower frequency. However, for the higher frequency, $\sigma^{\rm I}/\sigma$ is maximized at $k_0R = 2.2$ and follows a descending behavior after that point. This comes in stark contrast with the ascending behavior of $\sigma^{\rm I}/\sigma$ for the lower frequency.

In Fig. 16, we depict $\sigma^{\rm T}/\sigma$ and $\sigma^{\rm I}/\sigma$ versus k_0a_1 for different radii a_2 of the PEC core. A remarkable similarity is observed in the ISCS curves for all examined radii a_2. For $k_0a_1 < 2$, larger radii a_2 yield larger ISCS ratios, while, on the contrary, for $k_0a_1 > 4$, larger a_2 yield smaller ISCS ratios. Larger cores have larger ISCS ranges, e.g., for $a_2 = a_1/5$ we have $\sigma^{\rm T}/\sigma \in (0.35, 0.61), \sigma^{\rm I}/\sigma \in (0.1, 0.26)$ whereas for $a_2 = a_1/2$ we have that $\sigma^{\rm T}/\sigma \in (0.25, 0.7), \sigma^{\rm I}/\sigma \in (-0.15, 0.41)$. For $2 < k_0a_1 < 4$, a more steady behavior is observed. The ISCS are not significantly affected by the changes in the core's radius, except for the larger core $a_2 = a_1/2$, which yields larger variations. Both $\sigma^{\rm T}/\sigma$ and $\sigma^{\rm I}/\sigma$ exhibit more oscillatory behaviors for larger cores.

The variations of the ISCS ratios and values as well as the overall cross section and the sum of individual cross sections (denoted by $\hat{\sigma}$) for different distributions of $N = 4$ dipoles in the high-frequency zone are depicted in Fig. 17. The dipoles' distributions are those of the top panel of Fig. 15. A notable similarity is observed between the ISCS ratios and the values of all involved cross sections. For $k_0R > 2$ (i.e., when the

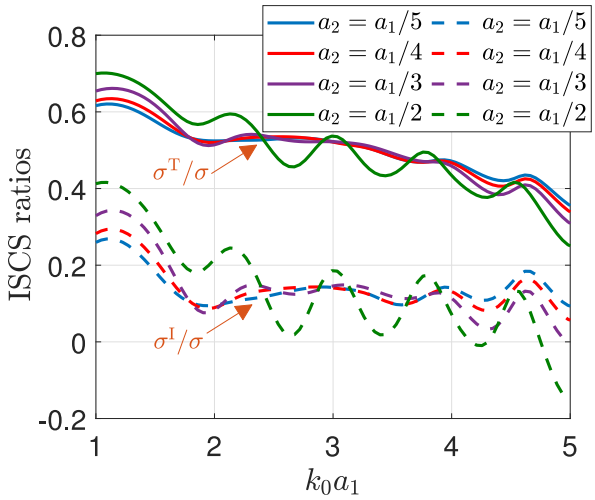

FIGURE 16. ISCS $\sigma^{\mathrm{T}}/\sigma$ and $\sigma^{\mathrm{I}}/\sigma$ versus the radius $k_0 a_1$ of a 2-layered sphere with $\epsilon_{r1} = 2$, $\mu_{r1} = 1.5$ and a PEC core of varying radius a_2, excited by $N = 4$ dipoles; two external ones at $r_0^1 = 1.3a_1$, $r_0^2 = 1.8a_1$ and two internal ones at $r_1^1 = 0.7a_1$, $r_1^2 = 0.9a_1$.

distance between the external and the internal dipole groups is larger than the sphere's diameter), the values and ratios begin to stabilize, which implies that the overall cross section σ develops a more stable behavior. Besides, all $\sigma^{\mathrm{T}}/\sigma$ ratios remain positive, except for $k_0R \in (1.25, 1.35)$ for $k_0a_1 = 10$. This fact is readily explained by the bottom panel, where we see that for these frequencies, the sum of individual cross sections is greater than the overall cross section.

In Fig. 18, we depict the same quantities as in Fig. 17, but in the low-frequency regime. The dipoles' distributions are those of the top panel of Fig. 15. The ISCS ratios and values remain very close for each of the two examined frequencies. The indirect ISCS remain negative for all k_0R; this fact implies that the interaction between the 0-excitation and 1-excitation fields, reduces the rate of the energy flux. Since the total ISCS remains positive, it is concluded that the sum of the 0- and 1-excitation cross sections is greater than the overall cross section but the sum of individual cross sections remains smaller than the overall cross section, as demonstrated by the bottom panel. Another interesting observation is the ascending behavior of the ISCS ratios as the distance k_0R between the dipoles' groups increases. Indirect ISCS values exhibit an ascending behavior as well–only steeper than their corresponding ratios. This is readily explained by the descending behavior of the total ISCS values with increasing k_0R. The contradiction between the ascending behavior of the indirect ISCS and the descending behavior of the total ISCS is explained from the bottom panel, where we see that the overall scattering cross section approaches zero for large distances R. Additionally, we see that the sum of the individual cross sections is very close to the overall cross section with both quantities following a similar descent pattern.

To explain the reduction of the energy flux rate, we point out that the overall energy flux is generated from the individual energy fluxes, which are quantified by the sum of the

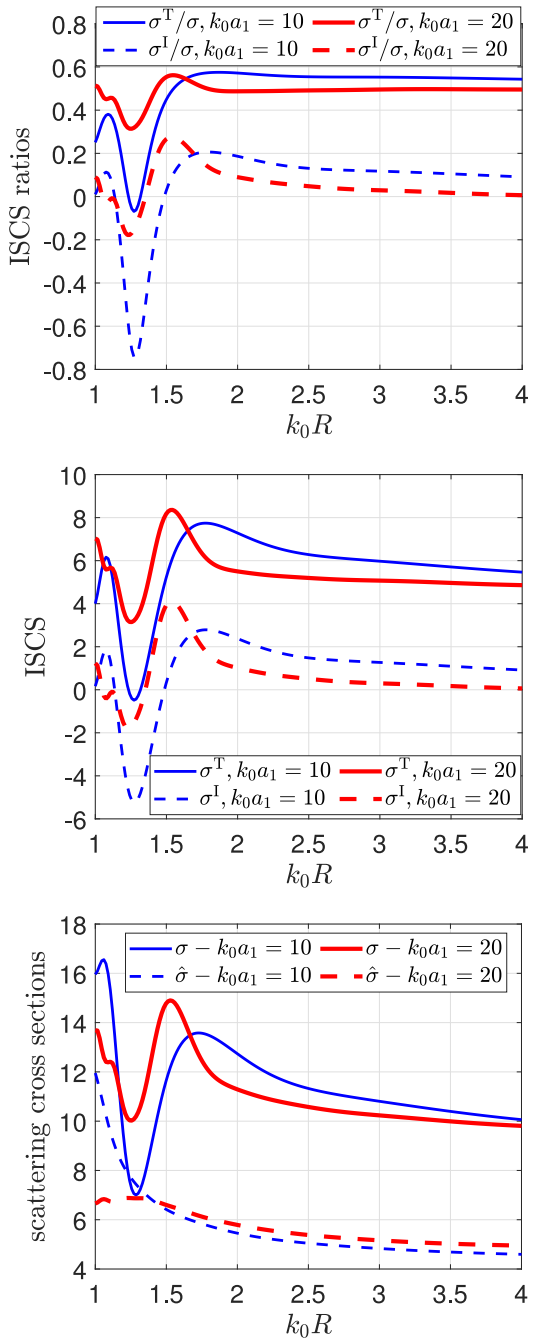

FIGURE 17. ISCS ratios and values versus k_0R for $k_0a_1 = 10$ and $k_0a_1 = 20$ (high-frequency zone) for a 2-layered scatterer with a dielectric core of $a_2 = a_1/10$ and parameters $\epsilon_{r1} = 2$, $\epsilon_{r2} = 3$, $\mu_{r1} = 1.5$, $\mu_{r2} = 2.5$. Excitation is due to $N = 4$ dipoles; two external ones and two in the first shell, all at varying distances R.

individual cross sections, and the energy flux caused by the interactions between the scattered fields, which are quantified by the total ISCS. Utilizing the Poynting vectors of the overall and individual fields, the Silver-Müller radiation condition (11) and the transmission boundary conditions (7) and (8) on S_1, we find that

$$\sigma = Z_0 \int_{S_1} \hat{\mathbf{n}} \cdot \mathbf{S}_1 \, ds(\hat{\mathbf{r}}), \tag{37}$$

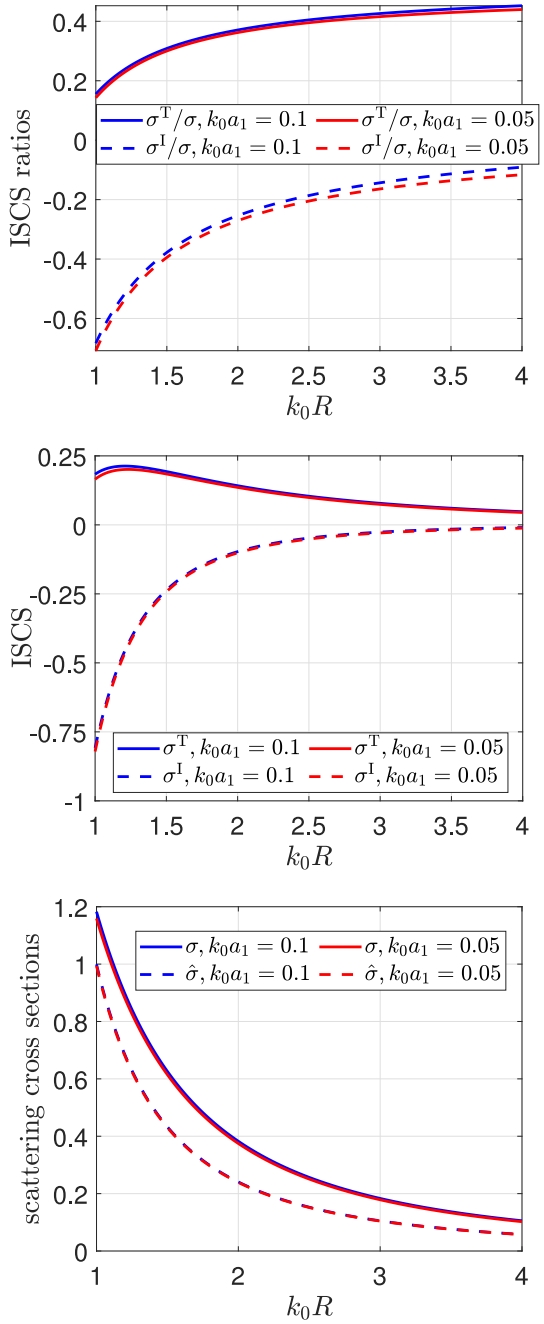

FIGURE 18. ISCS ratios and values versus k_0R for $k_0a_1 = 0.1$ and $k_0a_1 = 0.05$ (low-frequency zone), for a 2-layered scatterer with a dielectric core of $a_2 = a_1/10$ and parameters $\epsilon_{r1} = 2$, $\epsilon_{r1} = 3$, $\mu_{r1} = 1.5$, $\mu_{r2} = 2.5$. As in Fig. 17, the sphere is excited by $N = 4$ dipoles at varying distances R.

with $\mathbf{S}_1$ denoting the *overall energy flux* in V_1, and $Z_0 = \sqrt{\mu_0/\epsilon_0}$ the free-space impedance. From a physical standpoint, since σ is always positive, (37) shows that the overall scattering cross section is equal to the overall energy flow over all directions through the surface of the scatterer directed towards its exterior. By employing each individual Poynting vector $\mathbf{S}_1^j$, for $j = 1, \ldots, N$, using similar techniques as in the derivation of (37), and considering the definition (20), we obtain the following expression of the

TABLE 2. Scattering cross sections and ISCS, corresponding to the mixed excitation of a 2-layered dielectric spherical scatterer by $N = 4$ dipoles, for different radii of the core.

$k_0a_1 = 0.1$				
	$a_1 = 1.25a_2$	$a_1 = 2a_2$	$a_1 = 4a_2$	$a_1 = 10a_2$
σ_0^1	0.0320	0.0155	0.0118	0.0114
σ_0^2	0.0103	0.0051	0.0039	0.0037
σ_1^1	0.2776	0.1126	0.0284	0.0046
σ_1^2	0.5031	0.2045	0.0517	0.0083
σ_0	0.0786	0.0382	0.0292	0.0281
σ_1	1.5276	0.6206	0.1568	0.0251
σ^{T}	0.1299	0.0316	-0.0371	-0.0248
σ^{D}	0.7832	0.3211	0.0902	0.0253
σ^{I}	-0.6533	-0.2895	-0.1273	-0.0500
σ	0.9529	0.3693	0.0587	0.0032
$k_0a_1 = 2.5$				
	$a_1 = 1.25a_2$	$a_1 = 2a_2$	$a_1 = 4a_2$	$a_1 = 10a_2$
σ_0^1	5.4177	3.6491	4.7598	4.8296
σ_0^2	4.8377	3.5577	4.6977	4.7678
σ_1^1	7.4435	1.1752	0.2048	0.0196
σ_1^2	5.0671	1.3939	0.3361	0.0356
σ_0	19.3743	14.2296	18.7399	19.0205
σ_1	20.4900	4.7437	1.0450	0.1077
σ^{T}	46.3710	21.0969	15.0745	10.9368
σ^{D}	17.0983	9.1973	9.7864	9.4756
σ^{I}	29.2727	11.8996	5.2881	1.4611
σ	69.1370	30.8728	25.0730	20.5894
$k_0a_1 = 10$				
	$a_1 = 1.25a_2$	$a_1 = 2a_2$	$a_1 = 4a_2$	$a_1 = 10a_2$
σ_0^1	3.5664	2.6680	2.0767	2.2493
σ_0^2	3.3585	2.6080	2.0098	2.1824
σ_1^1	1.6721	1.1206	0.2805	0.0414
σ_1^2	3.4153	0.9268	0.2823	0.0534
σ_0	11.5605	9.5519	6.8774	7.5739
σ_1	5.0775	1.8499	0.7974	0.1788
σ^{T}	5.7787	5.8570	2.9373	3.7495
σ^{D}	4.6257	4.0785	3.0254	3.2262
σ^{I}	1.1530	1.7785	-0.0881	0.5234
σ	17.7910	13.1803	7.5866	8.2760

total ISCS

$$\sigma^{\mathrm{T}} = Z_0 \int_{S_1} \hat{\mathbf{n}} \cdot \mathbf{S}_1^{\mathrm{T}} \, \mathrm{d}s(\hat{\mathbf{r}}), \tag{38}$$

where $\mathbf{S}_1^{\mathrm{T}} = \mathbf{S}_1 - \sum_{j=1}^{N} \mathbf{S}_1^j$ denotes the *total interaction energy flux* in V_1. Eq. (38) implies that the total ISCS is equal to the energy flow through the surface S_1 of the scatterer, caused by the interactions between the individual fields in V_1. When $\sigma^{\mathrm{T}} > 0$, this energy flow is directed "outwards". However, when $\sigma^{\mathrm{T}} < 0$, (38) implies that the interactions between the participating fields, produce energy flow that is directed towards the interior of the scatterer ("inwards"), and, therefore, a portion of the energy flow returns back to the scatterer. This fact results in a reduction of the overall energy flux rate. We note, that $\sigma^{\mathrm{T}} < 0$ does not necessarily imply that all ISCS are negative; see Table 2, below, for $k_0a_1 = 0.1$ with $a_1 = 4a_2, a_1 = 10a_2$, where $\sigma^{\mathrm{T}}, \sigma^{\mathrm{I}} < 0$, but $\sigma^{\mathrm{D}} > 0$. Besides, a similar analysis to the above one is also

valid for the direct and indirect ISCS and their corresponding energy flows.

Table 2 presents the scattering cross sections and ISCS for the case where $N_0 = 2$ external dipoles, lying at $r_0^1 = 1.5a_1, r_0^2 = 2a_1$, and $N_1 = 2$ internal dipoles, lying at $r_1^1 = 1.01a_2, r_1^2 = 1.24a_2$, excite a 2-layered spherical scatterer with a dielectric core and $\mu_{r1} = 1.5, \mu_{r2} = 2.5$ and $\epsilon_{r1} = 2, \epsilon_{r2} = 3$. For the individual cross sections, we used the exact solution of the direct scattering problem for a single dipole [25], while for the rest of the cross sections involved, we used the optical theorems (22), (28) and (29). From the table, we see that all relations concerning ISCS are validated. Precisely, it holds: $\sigma = \sigma^{\mathrm{T}} + \hat{\sigma} = \sigma^{\mathrm{I}} + \sigma_0 + \sigma_1$ and $\sigma^{\mathrm{T}} = \sigma^{\mathrm{D}} + \sigma^{\mathrm{I}}$. In general, the findings of the figures and tables above suggest that the behavior of the total ISCS in the mixed excitation case is not easily predictable, since it is affected by various factors, like shells' thicknesses, core sizes, material parameters as well as external and internal dipoles distributions.

V. CONCLUSION

Excitation of a layered medium by N arbitrarily distributed magnetic dipoles was investigated. Two cases were considered and analyzed: *single layer excitation* when all dipoles lie in the same layer (or in the scatterer's exterior) and *mixed excitation* when dipoles are located in more than one layers. Interaction scattering cross sections (ISCS) were introduced which quantify the energy flux rate due to interactions between the individual and q-excitation fields by dipoles lying in the same layer or in different layers. Optical relations for the overall and q-excitation ISCS were derived. Physical bounds for the ISCS ratios, the number of excitation layers and the number of exciting dipoles were also established.

Numerical parametric analysis was performed for a layered spherical medium with a PEC or dielectric core, excited by 4 dipoles. From the presented numerical results, we concluded that the ISCS contribute significantly in the overall cross section. Therefore, when spherical waves excite a scatterer, the additivity of the cross sections must be examined with caution. Furthermore, we showed that in some cases the ISCS can also become negative; this was mainly observed for mixed excitation. In such cases, interactions of the participating fields may reduce the anticipated energy flux rate. Moderate changes in the geometrical characteristics of the medium do not result in significant changes of the ISCS ratios. Changes in the physical parameters of the medium affect significantly the ISCS ratios in the mixed excitation, but not so significantly in the single-layer excitation.

The ISCS ratios in external-excitation cases are very close to $1 - \frac{1}{N}$, especially in the low-frequency regime. For higher frequencies, the dipoles' strength is crucial for the ISCS ratios. Moreover, in higher frequencies, the established physical bounds can be used to determine accurately the medium's excitation layers and the number of exciting dipoles.

Finally, the distance of the excitation dipoles from the medium's boundary plays a pivotal role in the behavior of ISCS. For single-layer excitation, distributions away from the boundary yield larger values and more stable variations of the ISCS ratios–in contrast with distributions at close proximity to the boundary. For mixed excitation, the behavior of the ISCS is more erratic and depends on the scatterer's parameters and characteristics of the dipoles' distributions.

The presented numerical results in this work correspond to layered spherical scatterers. Examining the effect of the shells' shape on the ISCS is an interesting direction for future work. Spheroidal or ellipsoidal boundaries can be considered by developing combinations of analytical and numerical methodologies for the solution of the associated excitation problems by internal or external dipoles.

APPENDIX

Here we state relation (25) in the form of a theorem and prove it.

Theorem 1: The ratio $\tilde{\sigma}_q/\sigma_q$ of the q-interaction over the q-excitation cross section satisfies

$$1 - n_q \frac{\sigma_q^{\max}}{\sigma_q} \leq \frac{\tilde{\sigma}_q}{\sigma_q} \leq \min\left\{1 - n_q \frac{\sigma_q^{\min}}{\sigma_q}, 1 - \frac{1}{n_q}\right\}, \quad \text{(A.1)}$$

where $\sigma_q^{\max}, \sigma_q^{\min}$, respectively, denote the maximum and minimum individual cross sections of the dipoles lying in the excitation layer V_q.

Proof: For $\sigma_q^{\min}$ and $\sigma_q^{\max}$, we have

$$-n_q \sigma_q^{\max} \leq -\sum_{j=1}^{n_q} \sigma_q^j \leq -n_q \sigma_q^{\min}, \quad \text{(A.2)}$$

which, combined with the definition (17), yields

$$1 - n_q \frac{\sigma_q^{\max}}{\sigma_q} \leq \frac{\tilde{\sigma}_q}{\sigma_q} \leq 1 - n_q \frac{\sigma_q^{\min}}{\sigma_q}. \quad \text{(A.3)}$$

By the definition of the q-excitation cross section (15), we find

$$\sigma_q \leq \frac{1}{k_0^2}\left[\sum_{j=1}^{n_q} \int_{S^2} \left|\mathbf{g}_q^j(\hat{\mathbf{r}})\right|^2 \mathrm{d}s(\hat{\mathbf{r}})\right] + \frac{2}{k_0^2}\left[\sum_{j=1}^{n_q-1} \sum_{\nu=j+1}^{n_q} \left|\int_{S^2} \mathbf{g}_q^j(\hat{\mathbf{r}}) \cdot \overline{\mathbf{g}_q^{\nu}(\hat{\mathbf{r}})} \mathrm{d}s(\hat{\mathbf{r}})\right|\right]. \quad \text{(A.4)}$$

Hölder's inequality in conjunction with (14) and (A.4) imply

$$\sigma_q \leq \sum_{j=1}^{n_q} \sigma_q^j + 2 \sum_{j=1}^{n_q-1} \sum_{\nu=j+1}^{n_q} \left(\sigma_q^j\right)^{1/2} \left(\sigma_q^{\nu}\right)^{1/2}. \quad \text{(A.5)}$$

Now, since it holds

$$2\left(\sigma_q^j\right)^{1/2} \left(\sigma_q^{\nu}\right)^{1/2} \leq \sigma_q^j + \sigma_q^{\nu},$$

from (A.5), we get

$$\sigma_q \leq \sum_{j=1}^{n_q} \sigma_q^j + \sum_{j=1}^{n_q-1} \sigma_q^j (n_q - j) + \sum_{j=2}^{n_q} \sigma_q^j (j-1) = n_q \sum_{j=1}^{n_q} \sigma_q^j. \tag{A.6}$$

The last inequality together with (17) imply that

$$\frac{\tilde{\sigma}_q}{\sigma_q} \leq 1 - \frac{1}{n_q}. \tag{A.7}$$

Eq. (A.1) is derived from (A.3) and (A.7). Implication (26) is obvious.

Inequality $\sigma_q \leq n_q^2 \sigma_q^{\max}$, which is used in the derivation of (27), is a direct consequence of (A.6). Finally, relations (31), (32) as well as (35), (36), are proved by similar techniques.

REFERENCES

[1] G. Dassios, A. S. Fokas, and F. Kariotou, "On the non-uniqueness of the inverse MEG problem," *Inverse Problems*, vol. 21, no. 2, pp. L1–L5, Apr. 2005.

[2] G. Dassios and A. S. Fokas, "Electro-magneto-encephalography for a three-shell model: Dipoles and beyond for the spherical geometry," *Inverse Problems*, vol. 25, no. 3, Jan. 2009, Art. no. 035001.

[3] P. Gas, "Optimization of multi-slot coaxial antennas for microwave thermotherapy based on the S_{11}-parameter analysis," *Biocybern. Biomed. Eng.*, vol. 37, no. 1, pp. 78–93, 2017.

[4] T. Wang, G. Zhao, and B. Qiu, "Theoretical evaluation of the treatment effectiveness of a novel coaxial multi-slot antenna for conformal microwave ablation of tumors," *Int. J. Heat Mass Transfer*, vol. 90, pp. 81–91, Nov. 2015.

[5] B. Xu, M. Gustafsson, S. Shi, K. Zhao, Z. Ying, and S. He, "Radio frequency exposure compliance of multiple antennas for cellular equipment based on semidefinite relaxation," *IEEE Trans. Electromagn. Compat.*, vol. 61, no. 2, pp. 327–336, Apr. 2019.

[6] J. L. Hollmann and L. V. Wang, "Multiple-source optical diffusion approximation for a multilayer scattering medium," *Appl. Opt.*, vol. 46, no. 23, pp. 6004–6009, Aug. 2007.

[7] K. L. Wong, *Design of Nonplanar Microstript Antennas and Transmission Lines*. Reading, MA, USA: Wiley, 1999.

[8] R. Potthast, *Point Sources and Multipoles in Inverse Scattering Theory*. Boca Raton, FL, USA: Chapman and Hall/CRC, 2001.

[9] K. Yamatani, T. Ohe, and K. Ohnaka, "An identification method of electric current dipoles in spherically symmetric conductor," *J. Comput. Appl. Math.*, vol. 143, no. 2, pp. 189–200, Jun. 2002.

[10] X. Liu, B. Zhang, and J. Yang, "The inverse electromagnetic scattering problem in a piecewise homogeneous medium," *Inverse Problems*, vol. 26, no. 12, Oct. 2010, Art. no. 125001.

[11] H. Ammari, J. Chen, Z. Chen, D. Volkov, and H. Wang, "Detection and classification from electromagnetic induction data," *J. Comput. Phys.*, vol. 301, pp. 201–217, Nov. 2015.

[12] K. Wang, J. -J. Laurin, Q. Zhang, Q. Zhang, and K. Wu, "Three-dimensional scattering from uniaxial objects with a smooth boundary using a multiple infinitesimal dipole method," *IEEE Access*, vol. 8, pp. 80842–80854, 2020.

[13] C. T. Tai, *Dyadic Green Functions in Electromagnetic Theory*. Oxford, U.K.: IEEE-Press, 1994.

[14] A. Sommerfeld, *Partial Differential Equations in Physics*. New York, NY, USA: Academic, 1949.

[15] I. Lindell and A. Sihvola, *Boundary Conditions in Electromagnetics*. Hoboken, NJ, USA: Wiley-IEEE Press, 2019.

[16] G. Dassios and R. Kleinmann, *Low Frequency Scattering*. Oxford, U.K.: Clarendon Press, 2000.

[17] A. Kalogeropoulos and N. L. Tsitsas, "Excitation of a layered medium by N sources: Scattering relations, interaction scattering cross sections and physical bounds," *Quart. Appl. Math.*, vol. 79, no. 2, pp. 335–356, Jun. 2021.

[18] P. A. Martin, "Multiple scattering and scattering cross sections," *J. Acoust. Soc. America*, vol. 143, pp. 995–1002, Feb. 2018.

[19] M. I. Mishchenko and M. A. Yurkin, "Additivity of integral optical cross sections for a fixed tenuous multi-particle group," *Opt. Lett.*, vol. 44, no. 2, pp. 419–422, 2019.

[20] A. E. Moskalensky and M. A. Yurkin, "Energy budget and optical theorem for scattering of source-induced fields," *Phys. Rev. A*, vol. 99, May 2019, Art. no. 053824.

[21] C. Athanasiadis and N. L. Tsitsas, "Electromagnetic scattering theorems for interior dipole excitation of a layered obstacle," *Math. Methods Appl. Sci.*, vol. 30, no. 12, pp. 1467–1482, 2007.

[22] C. Athanasiadis, P. A. Martin, A. Spyropoulos, and I. G. Stratis, "Scattering relations for point sources: Acoustic and electromagnetic waves," *J. Math. Phys.*, vol. 43, no. 11, pp. 5683–5697, 2002.

[23] I. Liberal, I. Ederra, R. Gonzalo, and R. W. Ziolkowski, "Superbackscattering antenna arrays," *IEEE Trans. Antennas Propag.*, vol. 63, no. 5, pp. 2011–2021, Mar. 2015.

[24] N. L. Tsitsas and C. Athanasiadis, "On the scattering of spherical electromagnetic waves by a layered sphere," *Quart. J. Mech. Appl. Math.*, vol. 59, no. 1, pp. 55–74, 2006.

[25] N. L. Tsitsas, "Direct and inverse dipole electromagnetic scattering by a piecewise homogeneous sphere," *ZAMM J. Appl. Math. Mech.*, vol. 89, no. 10, pp. 833–849, Oct. 2009.

[26] P. Prokopiou and N. L. Tsitsas, "Electromagnetic excitation of a spherical medium by an arbitrary dipole and related inverse problems," *Stud. Appl. Math.*, vol. 140, no. 4, pp. 438–464, 2018.

[27] C. Gabriel, S. Gabriel, and E. Corthout, "The dielectric properties of biological tissues: I. Literature survey," *Phys. Med. Biol.*, vol. 41, pp. 2231–2249, Dec. 1996.

ANDREAS KALOGEROPOULOS was born in Xylokastron, Greece. He received the B.Sc. degree in mathematics from the University of Patras in 2012, under a scholarship, and the M.Sc. degree (Hons.) in applied mathematics from the Hellenic Open University in 2018. He is currently pursuing the Ph.D. degree with the School of Informatics, Aristotle University of Thessaloniki. His research interests include acoustic and electromagnetic scattering, inverse problems, and mathematical modeling.

NIKOLAOS L. TSITSAS (Senior Member, IEEE) was born in Athens, Greece, in 1979. He received the Diploma and Ph.D. degree in electrical engineering from the National Technical University of Athens (NTUA) in 2002 and 2006, respectively, and the M.Sc. degree in applied mathematics from the National and Kapodistrian University of Athens in 2005.

From 2008 to 2011, he was an Adjunct Lecturer with the School of Applied Mathematical and Physical Sciences, NTUA. From 2009 to 2011, he was an Adjunct Lecturer with the Hellenic Army Academy. Since 2012, he has been with the School of Informatics, Aristotle University of Thessaloniki, Greece, where he is currently an Associate Professor. He has authored or coauthored 62 papers in scientific journals and over 70 papers in conference proceedings. His research is focused on methodologies of applied mathematics in direct and inverse wave scattering and propagation theory.

Dr. Tsitsas is a member of the American Mathematical Society and the Technical Chamber of Greece, a Senior Member of the Optical Society of America, and an individual member of the Union Radio-Scientifique Internationale.